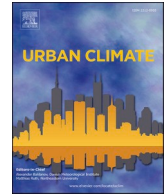




ELSEVIER

Contents lists available at [ScienceDirect](https://www.sciencedirect.com)

Urban Climate

journal homepage: www.elsevier.com/locate/uclim

Heat vulnerability and street-level outdoor thermal comfort in the city of Houston: Application of google street view image derived SVFs

YouJoung Kim^{a,*}, Dongying Li^a, Yangyang Xu^b, Yue Zhang^a, Xiaoyu Li^a, Lexi Muhlenforth^b, Shengliang Xue^a, Robert Brown^a

^a Department of Landscape Architecture and Urban Planning, Texas A&M University, College Station, TX, United States

^b Department of Atmospheric Sciences, Texas A&M University, College Station, TX, United States

ARTICLE INFO

Keywords:

City of Houston
COMFA energy budget model
Google street view image SVFs
Heat vulnerability assessment
And outdoor human thermal comfort

ABSTRACT

Heatwaves and urban heat islands disproportionately affect residents of urban areas. Past studies on the heat vulnerability indexes (HVI) to evaluate the heat-related risk have two major limitations: the inability to capture street-level human heat stress and reliance on single meteorological proxies to measure heat exposure. To address these gaps, this study examines the impact of street-level outdoor thermal comfort (OTC) on heat vulnerability in the city of Houston, Texas. OTC refers to an individual's thermal perception of their surroundings. The study estimates the impacts of HVI scores and energy budget (EB) values of OTC on heat-related disease while investigating their spatial distributions and clusters. The results show that the explanatory power of the suggested models on the number of emergency department (ED) visits improved when the street-level OTC had higher HVI scores and more comfortable conditions. A positive bivariate relationship was found between the HVI scores and EB values, showing the highest explanatory power (adj-r2) of around 36%. Chronic disease and heat exposure significantly affected the HVI, whereas tree and sky view factors were crucial determinants of the EB values. These findings provide a new approach to heat vulnerability evaluation at the human scale to effectively address heat-related risk.

1. Introduction

Heatwaves and urban heat islands (UHI) disproportionately affect residents of urban areas. The rising temperature is directly related to recent increases in heat-related mortality and morbidity (Niu et al., 2021). Heat-related illnesses are often concentrated in specific segments of the population, such as those comprising low-income, uneducated, elderly, and unhealthy individuals (Uejio et al., 2011; Ellena et al., 2019, 2020). According to the population vulnerability framework (Barros et al., 2014; Brooks, 2003; Crimmins et al., 2016), Heat Vulnerability are often conceptualized as consisting of three components: exposure, sensitivity, and adaptability. To examine the uneven distribution of heat-related risks and identify vulnerable populations, numerous attempts have been made to

* Corresponding author at: Landscape Architecture and Urban Planning, Texas A&M University, College Station, TX 77840, United States of America.

E-mail addresses: kyj0244k@tamu.edu (Y. Kim), dli@arch.tamu.edu (D. Li), yangyang.xu@tamu.edu (Y. Xu), yz94@tamu.edu (Y. Zhang), lxy819457986@tamu.edu (X. Li), lmuhlenforth@tamu.edu (L. Muhlenforth), simonxue92@tamu.edu (S. Xue), rbrown@arch.tamu.edu (R. Brown).

<https://doi.org/10.1016/j.uclim.2023.101617>

Received 3 October 2022; Received in revised form 17 June 2023; Accepted 17 July 2023

2212-0955/© 2023 Elsevier B.V. All rights reserved.

produce validated heat vulnerability indexes (HVIs) (Niu et al., 2021; Chen et al., 2022; Karimi et al., 2018; Sun et al., 2021). These studies produced meaningful implications in that reporting major socio-economic and built-environment drivers of such vulnerability to guide policy development and resource allocation in preparation for and response to heat-related risks.

Numerous efforts have been made to construct a heat vulnerability index to identify the heat-related public health risk. With growing concerns of negative impact of heat waves on health, several studies focused on investigating socio-economic population characteristics, heat stress exposure, and accessibility to medical resources while exploring their interaction with the environment in identifying heat vulnerability (Romero-Lankao et al., 2012; Ellena et al., 2020; Niu et al., 2021). The varying association between vulnerability index scores and heat-related disease has been thoroughly explored in multiple studies (Loughnan et al., 2014; Eisenman et al., 2016; Nayak et al., 2018). However, those past studies have a significant limitation in that they mostly use all-cause morbidity or mortality as the outcome in their index construction (Krstic et al., 2017; Conlon et al., 2020; Cheng et al., 2021). This is not suitable as a proxy for heat-related disease as a variety of factors may impact in addition to heat-related risks.

Despite the importance of HVIs, two major limitations hinder index refinement and translations of the indexes into policy implication. Firstly, HVIs were mostly developed for the scales of aggregated areal-based units, such as census tracts (Cheng et al., 2021). Such zonation may entail the modifiable areal unit problem (MAUP) (Openshaw, 1981) and the uncertain geographic context problem (UGCoP) (Kwan, 2012). In particular, as humans' heat exposure is determined by the immediate surroundings, environmental and sociodemographic factors aggregated to arbitrary administrative boundaries may not capture heat-related health risks (Karanja and Kiage, 2021; Mushore et al., 2018). Therefore, assessment of spatially explicit heat exposure factors at the street level is needed to accurately capture human heat-related risks. Secondly, existing HVIs rely on single meteorological (e.g., surface temperature, air temperature) or environmental proxies (e.g., vegetation index, impervious surface) to measure heat exposure (Ellena et al., 2020). However, such a simplified method does not take into consideration the multiple energy balance fluxes that occur during human-environment exchanges and human physiological responses to thermal stress. Due to these two limitations, HVIs often exhibit limited capabilities in explaining the variances in heat-related mortality or morbidity (Harlan et al., 2013; Conlon et al., 2020), which hinders policy formulation.

This study aims to explore street-level outdoor thermal comfort (OTC) in order to determine the spatial distribution of heat vulnerability. Specifically, we investigated the impact of heat vulnerability components on the occurrence of heat-related diseases, while considering spatial clusters of street-level OTC hot spots. To achieve this goal, we pursued three primary objectives. First, we assessed the spatial distributions of Heat Vulnerability Index (HVI) scores and street-level OTC to pinpoint areas vulnerable to thermal stress, while identifying the major indicators of vulnerability distributions. Second, we explored the correlation between HVI scores and street-level OTC to determine the spatial clusters of heat vulnerability hot spots, driven by outdoor thermal conditions and physical features of the street environment. Lastly, we estimated the impacts of heat vulnerability and street-level OTC on heat-related diseases while exploring the predictive performance of suggested HVI in explaining the variation of heat-related disease. Particular attention was given to the changes in the effect of heat vulnerability components according to the different levels of OTC. The city of Houston was selected as the study region due to its high records of heat-related illnesses, sociodemographic diversity, and increasing risks of Urban Heat Island (UHI) effects. Our study findings offer a new approach to heat vulnerability evaluation by measuring heat exposure at the human scale and offer decision support with resource allocation to effectively address heat risk in the age of climate change.

2. Literature review

2.1. Heat vulnerability and heat-related morbidity/mortality

With growing concerns of negative impact of heat waves on health, research has focused on human thermal regulation and its interaction with the environment in identifying heat vulnerability. Various definitions and operation frameworks of vulnerability have been proposed (Cheng et al., 2021; Niu et al., 2021). For example, some definitions focus on assessing the probability of risk exposure, while others emphasize the population's health state preceding or following disasters (Karanja and Kiage, 2021; Lee, 2014). One widely accepted conceptualization defines heat vulnerability as the level of vulnerability to heat across geographic space, thus identifying the population most in need of intervention (Reid et al., 2009). In this study, we adopt the population vulnerability framework (Barros et al., 2014; Brooks, 2003; Crimmins et al., 2016), which posits that the situational risks (i.e., the risk that are context- and temporary dependent, rather than related to individual factors) are high if the exposure to heat is high, the sensitivity of the population/system is high, and the adaptive capacity is low (Cheng et al., 2021).

Heat vulnerability is linked to demographic and socio-economic factors, built environment features, pre-existing health conditions, and air conditioning prevalence. Demographic and socio-economic status characteristics include poverty, employment, education, income, gender, age, and minority status (Reid et al., 2009; Johnson et al., 2012; Sharma et al., 2018). The built environment also affects vulnerability through urban form, greenery, and housing quality, which determine the heat exposure level of indoor and outdoor conditions (Uejio et al., 2011; Harlan et al., 2013; Sharma et al., 2018). Individuals with pre-existing health conditions, such as cardiovascular, respiratory, diabetes, kidney, and neurological conditions, are particularly vulnerable to the impacts of heat (Prudent et al., 2016; Sharma et al., 2018). Air conditioning can reduce heat vulnerability by providing access to cool indoor environments, especially for vulnerable populations. However, relying on air conditioning without considering energy efficiency or equitable access may contribute to increased energy consumption, environmental impacts, and disparities in heat resilience (Bradford et al., 2015; Sharma et al., 2018).

Although heat vulnerability indexes are constructed to reveal public health risks, previous studies have found varying associations between the index scores and mortality and morbidity outcomes. For example, Kim et al. (2017) developed an HVI that explained 32%

of the observed heatwave-related deaths in 232 administrative counties in Korea. Loughnan et al. (2014) compared the performance of HVI in predicting emergency service demand across different regions and found that the index score explained between 18.6% and 80.7% of variability in the outcome (Loughnan et al., 2014). The variations in the explanatory power of HVI across the above-mentioned and other studies alike may be explained by spatial/temporal scales, population differences, variations in indicator selection, index construction, and validation dataset. For example, many studies used all-cause morbidity or mortality as the outcome, which may be impacted by a variety of factors in addition to heat-related risks (Loughnan et al., 2014; Conlon et al., 2020; Cheng et al., 2021). In particular, two limitations of existing HVI indexes related to scale mismatch and poor proxies of heat exposure should be noted.

HVIs were mostly developed at the scales of administrative boundaries such as counties or census tracts (Romero-Lankao et al., 2012; Ellena et al., 2020). Results from such areal-based boundaries may be subject to aggregation fallacy, where the results vary greatly depend on the level of aggregation. In addition, by measuring the environmental exposure at the county or tract level, it is assumed that such spatial context reflects the external stressors that people residing in this area experience. However, this assumption is subject to the uncertain geographic context problem (UGCoP), which states that the areal units deviate from the actual geographic context that affect people's behaviors and health outcomes. The spatial variations of the street's thermal conditions that people use most frequently for outdoor activity and movements are not captured. To address this issue, assessment of spatially explicit heat exposure factors at the street level is needed to accurately capture human heat-related risks.

Another major limitation of existing HVI indexes is related to the use of environmental (e.g., vegetation index, impervious surface) or meteorological factors (e.g., surface temperature, air temperature) as proxies for human thermal stress (Cheng et al., 2021). The variables frequently adopted for measuring heat exposure are land surface temperature, air temperature, relative humidity, and wet-bulb globe thermometer WBGT (Cheng et al., 2021) (See Appendix Table 1 for a table of the detailed variables and example studies). These are quantified according to their intensity (e.g., daily maximum, minimum, and mean), duration (e.g., heat waves and tropical night days, defined as days with temperatures over a certain threshold), variance (e.g., temperature range), and frequency (Romero-Lankao et al., 2012). Although meteorological factors are considered powerful determinants of heat vulnerability (Ellena et al., 2020; Niu et al., 2021; Cheng et al., 2021), such a simplified method does not take into consideration the multiple energy balance fluxes during human–environment exchanges and human physiological responses to thermal stress. As such, the results often fail to reflect the actual thermal sensations people feel when they are in the environment. These two limitations often result in inaccurate and biased estimations of urban residents' heat hazard exposure. Accordingly, it is increasingly required to explore the potential applicability for street-level human outdoor thermal comfort in the vulnerability assessment by presenting the actual thermal sensations of urban residents at the street scale.

2.2. Heat exposure and outdoor thermal comfort

Differing from heat indices that combine only weather factors (Anderson et al., 2013), human thermal indices can take into account the full spectrum of ambient, physiological, and physical activity conditions that affect human–environment heat transaction (de Freitas and Grigorieva, 2015). Heat stress modeling is critical for population health risk characterization because it strongly predicts heat-related mortality or morbidity. A 10% increase in Physiological Equivalent Temperature (PET) (Höppe, 1999) or Universal Thermal Climate Index (UTCI) (Bröde et al., 2012) is associated with a 3%–5% increase in the probability of heat-related death with a 1–3 day lag (Nastos and Matzarakis, 2012). Beyond heat exhaustion, heat stroke, and other diseases caused by heat, indices such as PET also proved to be important indicators of population-level cardiovascular, respiratory, and renal diseases, both directly and through other mediators such as air pollution and microbiota diversity (Dastoorpoor et al., 2021; Goldie et al., 2018; Jayasekara et al., 2019; Rainham and Smoyer-Tomic, 2003).

Among all thermal index models, outdoor thermal comfort (OTC) indices refers to the actual thermal sensations that people feel outdoors (Kumar and Sharma, 2020). According to the ANSI/ASHRAE Standard 55 (2017), it is defined as “the condition of mind, which expresses satisfaction with the thermal environment.” However, its determinants are not limited to the psychological status but also include meteorological, physiological, and physical conditions (Chen and Ng, 2012; Cocco et al., 2016). To date, >165 different outdoor thermal comfort indexes have been developed worldwide to quantify outdoor human thermal comfort accounting for human physiology (Potchter et al., 2018). Several studies have confirmed that OTC indexes are stronger indicators than single meteorological factors in predicting heat-related illnesses, behavioral thermal response, and physiological thermal adaptation (Ohashi et al., 2014; Kim and Brown, 2022).

COMFA (Comfort Formula) is a validated thermal comfort model that evaluates the thermal sensation of people in outdoor environments (Brown and Gillespie, 1986). It was developed to incorporate human–environmental heat exchange and to consider microclimate effects on human thermal comfort, and it has been applied in various studies performing thermal exposure assessments (Correa et al., 2012; Li et al., 2022; Vanos et al., 2019; Kim and Brown, 2021). COMFA considers a person's metabolic energy, absorbed solar and terrestrial radiation, emitted terrestrial radiation, and convective and evaporative heat exchange in their estimation of outdoor thermal comfort. Several studies adopting and refining the COMFA model added additional adaptability factors, including physical activity and clothing choices (Kenny et al., 2009; Vanos et al., 2012). A unique advantage of the model is that it outputs result in energy flux (W/m^2) as a measurement of the total energy budget of a person and further partitions the result into individual fluxes.

In this study, the COMFA model was chosen due to its ability to assess street-level outdoor thermal comfort based on street morphological features. Using the energy flux principle and the SVF parameter, the model can distinguish individual physical components of the built environment and evaluate their contributions to thermal loadings on the human body. This approach enables the capture of spatial variations in outdoor thermal comfort, which are modified by street-level environmental features, with high

accuracy and validity. Therefore, through the use of the COMFA model, the amount of radiative thermal stress people receives from the sky and ground, respectively, when walking along the observed street spots, as well as the amount of solar radiation and terrestrial radiation absorbed by people, can be estimated.

2.3. Assessing street solar geometry using Google Street View imagery

Recent advancements in utilizing Google Street View imagery for street-level environmental assessments make it possible to capture fine-scaled ambient features and mass-process the data for large study areas (Anguelov et al., 2010; Rundle et al., 2011). State-of-the-art image recognition and segmentation approaches can be employed to identify objects and elements in studies quantifying the amount of sky, building, and greenness in urban areas; assessing urban street morphology and composition; and evaluating perceptions and behaviors (Lu, 2019; Middel et al., 2019; Rossetti et al., 2019).

One measure that can be derived from GSV is Sky View Factors (SVFs), which is a measurement of the proportion of the sky that is visible from the ground (Bernard et al., 2018; Oke, 1981). It is a key determinant of street-level outdoor thermal comfort in that it controls the amount of solar radiative energy a person can receive at a given location, which is modified by street trees, buildings and ground pavement (Kim and Brown, 2022; Kim et al., 2022). Therefore, its values are significantly associated with surface energy balance, local air circulation and outdoor thermal comfort (Middel et al., 2019). The less shade, the greater the SVF, which leads to increased daytime and decreased night-time air temperature (Yan et al., 2014; Yuan and Chen, 2011) and an increase in human thermal discomfort and heat risk (Lin et al., 2013). For densely developed urban areas, outdoor thermal comfort would be highly varied spatially and temporally according to the SVFs values due to the high complexity of urban street geometry. This implies that for street-level outdoor thermal comfort estimation and street-level heat vulnerability assessment, particularly for census or block-level scale, SVFs should be incorporated in their heat exposure estimation process for finer spatial scale resolution.

In summary, sufficient studies haven't been undertaken to measure heat hazards and link to policy planning. Despite surging interests in conducting HVI studies, current challenges related to HVI centers around the spatial scale mismatches, and the omission of biophysiological processes that underly human-environment energy exchange and heat adaptation. Thereby, in-depth analysis of human heat exposure using outdoor human thermal comfort models that consider human physiology and thermal adaptation is necessary. This study utilizes thermal index models enhanced by SVF values derived from GSV images to examine how areal HVI scores are modified by levels of outdoor thermal comfort conditions, as well as their joint effects in determining heat-related healthcare facility utilization.

3. Materials and methods

3.1. Study area

Houston, a large metropolis in Southeast Texas, is an ideal study area due to its intensifying urban heat island (UHI) effect and increasing risk of heat-related illnesses. It is home to 2.3 million residents with a population density of 1389/km². Houston has a humid subtropical climate with tropical influences, with the warmest month being August at 34.7 °C and the coldest month being January at 5.7 °C (<https://www.weather.gov>). The UHI effect, often around 1.7 °C, can peak at up to 3.3 °C due to urban expansion associated with growing population and high development density (Streutker, 2003; Conlon et al., 2020). Heat mortality is expected to increase by up to 200% for all Representative Concentration Pathway (RCP) and Shared Socioeconomic Pathway (SSP) scenarios compared to a historical reference period spanning 1991–2010 (Marsha et al., 2016).

3.2. Development of heat vulnerability index (HVI)

We conducted an ecological study at the census tract level, with exposure and outcome datasets from multiple sources (See Fig. 2). The meteorological datasets were obtained from GridMet, a downscaled weather prediction modeling dataset. The Landsat 8 and Sentinel 2 remote sensing images were collected to measure the land surface temperature (LST) and normalized difference vegetation index (NDVI). The Sky View Factor (SVF) was quantified using AI algorithm-driven Google Street View Image analysis. The COMFA model was applied to estimate physiological outdoor thermal comfort of a person using collected meteorological variables and Sky View Factors (SVFs) inputs. The Social Vulnerability Index (SoVI) algorithm and Spatial regression analysis were employed for the variable reduction in constructing HVI and evaluating predictive performance of selected heat vulnerability components, respectively.

3.2.1. Indicator extraction and processing

1) Heat exposure and built-environment variables.

Meteorological data and satellite imageries were obtained as heat exposure proxies and utilized as inputs for outdoor thermal comfort estimation. Meteorological data were obtained from the GridMET (Abatzoglou, 2013) produced by the Climatology Lab (<https://www.climatologylab.org/gridmet.html>). The data were compiled by interpolating regional reanalysis data using NLDAS-2 with gridded climate data from the Parameter-elevation Regressions on Independent Slopes Model (PRISM). PRISM has a native resolution of 800 km but is filtered down to 4 × 4 km gridded data to allow for easier access (PRISM Climate Group, 2014). GridMET provides ~4 km resolution variables such as maximum and minimum daily temperature, precipitation amount, downward surface

Table 1
Summary of HVI indicators (unit, source and description).

	Category	Variable	Unit	Source	Description
Exposure	Heat hazard	Daytime thermal comfort	W/m2	Climatorology lab	Estimated daytime energy budget using COMFA model - 3 years of averaged daily Max Ta & Slr & Ws, averaged daily Min Rh, Slr = 980 w/m2
	Heat hazard	Nighttime thermal comfort	W/m2	Climatorology lab	Estimated nighttime energy budget using COMFA model - 3 years of averaged daily Min Ta & Ws, averaged daily Max Rh, Slr = 0 w/m2
	Heat hazard	Compared heat index	–	See appendix	See appendix section
	Bult environment	Sky view factors	%	Google API database	Derived from Hemispherical - Google street view iamge (GSV), Total N = 10,000 (primary = 7000 / secondary = 3000)
	Bult environment	Tree view factors	%	Google API database	Derived from Hemispherical - Google street view iamge (GSV), Total N = 10,000 (primary = 7000 / secondary = 3000)
	Bult environment	Building view factors	%	Google API database	Derived from Hemispherical - Google street view iamge (GSV), Total N = 10,000 (primary = 7000 / secondary = 3000)
	Bult environment	Normalized difference vegetation index	–	USGS	Sentinel 2 satllite image, Daytime - 3 days (2020-08-04, 2019-09-14, 2020-07-06,), cloud cover <3%
Sensitivity	Bult environment	Land use	%	NLCD	National Land Cover Database (30*30 m) resolution)
	Pre-existing health condition	Uninsured	%	BRFSS, CDC	Model-based estimate for crude prevalence of current lack of health insurance among adults aged 18–64 years
	Pre-existing health condition	Hypertension	%	BRFSS, CDC	Model-based estimate for crude prevalence of high blood pressure among adults aged ≥ 18 years
	Pre-existing health condition	Asthma	%	BRFSS, CDC	Model-based estimate for crude prevalence of current asthma among adults aged ≥ 18 years
	Pre-existing health condition	Diabetes	%	BRFSS, CDC	Model-based estimate for crude prevalence of obesity among adults aged ≥ 18 years
	Pre-existing health condition	Obesity	%	BRFSS, CDC	Model-based estimate for crude prevalence of diagnosed diabetes among adults aged ≥ 18 years
	Demographic	population density	Per Sq. Mile	ACS 2018 (5-Year Estimates)	Population density
	Demographic	age_under5	%	ACS 2018 (5-Year Estimates)	population under 5 Sears
	Demographic	age_65over	%	ACS 2018 (5-Year Estimates)	population 65 years and over
	Demographic	non_White	%	ACS 2018 (5-Year Estimates)	population other than White
Adaptive capacity	Demographic	Hispanic_Latino	%	ACS 2018 (5-Year Estimates)	Hispanic or Latino population
	Social isolation	Living Alone	%	ACS 2018 (5-Year Estimates)	Householder living alone
	Social isolation	Living Along_65over	%	ACS 2018 (5-Year Estimates)	Householder 65 years and over, and living alone
	Social isolation	English Ability_not Well	%	ACS 2018 (5-Year Estimates)	Language Spoken at Home not well or not at all
	Social isolation	disability	%	ACS 2018 (5-Year Estimates)	Population with disability
	Socio-economic status	less_highSchool	%	ACS 2018 (5-Year Estimates)	Population 25 years and over, and less than high school
	Socio-economic status	below_povertLevel	%	ACS 2018 (5-Year Estimates)	Ratio of Income in 2018 to Poverty Level under 1.0
	Socio-economic status	Unemployment	%	ACS 2018 (5-Year Estimates)	Unemployed
	Socio-economic status	FemHousHold	%	ACS 2018 (5-Year Estimates)	Females head of household
	Mobility	No vehicle	%	ACS 2018 (5-Year Estimates)	Households without vehicle
Building & housing quality	Home amenity	AC prevalence	%		
	Building & housing quality	Units_perSqmi	Count/sq. mile	ACS 2018 (5-Year Estimates)	Housing units
	Building & housing quality	buildingAge_before1970	%	ACS 2018 (5-Year Estimates)	Year structure built before 1970
Building & housing quality	buildingAge_before1980	%	ACS 2018 (5-Year Estimates)	Year structure built before 1980	

* BRFSS, CDC, ACS, USGS, NLCD.

shortwave radiation, wind velocity, and relative humidity. The data used in this study span from 2018 to 2020 and cover the City of Houston.

Satellite imagery data were acquired to estimate Land Surface Temperature (LST) and the Normalized Difference Vegetation Index (NDVI) (See Fig. 3). The Landsat 8 OLI/TRIS images, preprocessed by the USGS, were used to calculate LST with a 30-m spatial resolution. Four imageries retrieved using the Radiative Transfer Equation (RTE) method were selected based on three criteria (See Appendix Eq. 1): <10% cloud cover, sunny days with no prior precipitation, and images with no scan errors taken during July or August between 2018 and 2020. Sentinel-2 Level 1 imagery, obtained from ESA's Copernicus Open Access Hub, was used to calculate NDVI. NDVI is an indicator used to evaluate the density of green healthy vegetation, calculated as the ratio between top-of-atmosphere reflectance of a red band around 0.66 μm and a near-infrared (NIR) band around 0.86 μm . The spatial resolution of the Sentinel-2 imagery was 30 m, matching the Landsat 8 data. The collection dates of Sentinel-2 imageries were close to the Landsat 8 imagery's capture dates during July or August between 2018 and 2020.

Air conditioning and Housing quality data were collected as adaptive capacity proxies. Air conditioning data obtained from the Harris County Appraisal District (HCAD) were utilized, which describes the types of cooling systems in the structures of each parcel in Houston. This variable specified whether there is central air conditioning (A/C) and whether there is any A/C. For each parcel, we considered A/C available if at least one structure has A/C (as it is common for sheds and other storage structures to be built on a property). We then calculated the percentage of parcels with A/C and central A/C at the census tract level. Regarding housing quality, we utilized the following data from the 2018 5-year American Community Survey reflecting the housing quality at the census tract level: housing units, the proportion of structures built before 1970, and the proportion of structures built before 1980 (United States Census Bureau, 2019).

2) Demographic and chronic disease variables.

Demographic data at census tract level were obtained from the 2018 5-year American Community Survey. These include population density, land area, the proportion of the population aged under 5 years, the proportion of the population aged 65 years and over, the non-White proportion of the population, the Hispanic or Latino proportion of the population, the proportion of householders living alone, the proportion of householders aged 65 years and over and living alone, the proportion of the population without a high school diploma, the proportion of the population living in poverty, the proportion of the population with disability, the proportion of the population that is unemployed, the proportion of households without vehicles, and the proportion of householders that are female (United States Census Bureau, 2019).

Census tract level pre-existing chronic disease factors were collected from the report released by the Behavioral Risk Factor Surveillance System (BRFSS) of the Centers for Disease Control and Prevention (CDC) in 2019. The pre-existing chronic disease measures we used were estimated crude prevalence of high blood pressure, asthma, obesity, and diagnosed diabetes among adults, as well as the estimated rate of lack of health insurance among adults (Centers for Disease Control and Prevention, 2019).

3) Heat-related disease data.

Emergency department (ED) visit data between January 2016 and June 2021 were obtained from the Texas Center for Health Statistics, Department of State Health Services. This dataset includes inpatient and outpatient records from approximately 500 hospitals or facilities in Texas coded based on the International Classification of Diseases, 10th revision (ICD-10). Due to data sharing and confidentiality constraints, patients' geographic information was only released at the zip code level, and dates of visits were unavailable. To identify heat-related ED visit, we selected records that had diagnoses belonging to T67 (effects of heat and light) and X30 (exposure to excessive natural heat) classifications, which covered heat stroke, heat syncope, heat cramp, heat exhaustion, heat fatigue, heat edema, and other unspecified diseases due to effects of heat. We then computed counts at the level of zip code tabulation area (ZCTA) and calculated the population-weighted counts using census tracts as units, by identifying ZCTAs that intersect with each census tract and deriving weighted average by population. Data extraction and preparation were conducted in R.

3.2.2. HVI construction

To measure the heat vulnerability in the city of Houston, we constructed an HVI to assess the multi-dimensional aspects of community vulnerability, which included heat exposure, sensitivity, and adaptive capacity. The index was developed to reveal the unequal spatial distribution of heat vulnerability at the census tract level and how it was associated with street-level outdoor thermal comfort conditions. The five heat vulnerability components were identified using the principal components analysis (PCA): chronic disease, heat exposure, social isolation, street features, and AC prevalence. Census tracts were chosen as the primary spatial reference unit for our index construction and vulnerability evaluation. The following three major steps were taken for HVI construction.

First, the potential variables necessary for vulnerability proxies were obtained from publicly available demographic, socio-economic, and spatial data at the census tract levels. At the initial stage, 31 variables were acquired and compiled in terms of heat exposure, sensitivity, and adaptive capacity indicators from BRFSS, CDC, ACS, USGS, and NLCD (Table 1). After all the data were computed and normalized, 15 variables were derived and selected for heat vulnerability construction after testing for multicollinearity among the variables.

Second, to construct the heat vulnerability index, principal component analysis was used as a primary statistical method to reduce the dimensionality of the datasets. This technique minimizes the number of original variables that load highly on any one factor and increases the variation among factors. Accordingly, it helps to identify dominant factors determining heat vulnerability. We retained

the five factors that had eigenvalues greater than one. The eigenvalue represents the concentration of variability in a correlation matrix. Thus, we choose the factor with the highest eigenvalue to include the maximized variability in our model. The Kaiser-Meyer-Olkin (KMO) measure of sampling adequacy was used to check data suitability for PCA and exclude the variables with KMO values smaller than 0.5. The identified five factors are described in Table 2, and the title of each component is given according to the dominant variables with a higher coefficient of factor loadings for each component group.

Lastly, the five components were aggregated into a single measurement unit to present an overall score of heat vulnerability for each census tract. For indicator composition, this study adopted an additive model (or un-weighted quotative aggregation) suggested by Cutter et al. (2003), which assumes all components are equally important and linearly related to the overall sum. Additionally, to estimate the impact of HVIs values on heat-related disease, the multivariate statistical techniques were selected (Harlan et al., 2013; Conlon et al., 2020). As a proxy for the dependent variable, the number of heat-related emergency department visits were used. Specifically, spatial lag models were chosen for producing regression coefficients as weighting values to control the spatial dependency.

3.2.3. Statistical analysis

Cluster analysis and spatial regression analysis were conducted based on the HVI scores and street-level outdoor thermal comfort (OTC) values. For the cluster analysis, the Bivariate Local Indicator of Spatial Association (LISA) cluster was used to map the hot spots of HVI and street-level OTC of the targeted study area at census tracts. Using the local Moran’s I value, LISA provides the statistic of spatial association for each location with an assessment of significance while estimating a proportional relationship between the sum of the local statistics and a corresponding global statistic (Anselin, 2002). This analysis is mainly performed using ArcMap and Geoda software.

The associations between HVI, street-level outdoor thermal comfort (OTC), and heat-related disease were estimated using spatial lag models. Specifically, we focused on the effects of heat vulnerability components on the number of emergency department (ED) visits according to the different levels of street-level OTC. To achieve this, three separate models of two groups were generated for all levels, including high-level (hot spots) and low-level (cold spots) OTC, to reveal the changes in the vulnerability impacts related to street-level OTC. The spatial lag model (SLM) was employed because the Moran’s I test observed a significant spatial autocorrelation in their datasets. This regression method postulates that the residuals could be a result of autocorrelation in the dependent variable while dealing with spatial interaction issues and heterogeneity in residuals of regression models (Paelinck, 1978; LeSage, 2008). A series of statistical tests – Akaike Information Criterion (AIC) / Bayesian Information Criterion (BIC) test, and Lagrange Multiplier (LM) tests – were also performed for model selection and development.

3.3. Estimation of outdoor human thermal comfort (OTC)

3.3.1. COMFA energy budget model

The COMFA (Comfort Formula) model was selected to estimate the physiological thermal comfort, which serves as the exposure indicator of our heat vulnerability model. It is described as follows:

$$E = M + R - C - K - \Delta S \tag{1}$$

where ΔS is the change in heat storage (W/m²), which is equal to zero at energy balance, above zero at energy surplus, and below zero at energy deficit, with the major energy streams being convective heat loss (C), evaporative heat loss (E), conductive heat loss (K), radiative exchanges (R), and metabolic heat production within the body (M) (Brown and Gillespie, 1986; Vanos et al., 2012). We used basic COMFA parameter settings that included a metabolic rate of a walking person of 190 W/m², at a standard walking speed of 1.4 m/s, and summer clothing insulation (T-shirt, short pants, socks, running shoes; clothing resistance (s/m) of 32.78; and clothing vapor resistance (s/m) of 46.46).

3.3.2. Google Street View Image-derived SVFs

GSV2SVF, an interactive GIS tool, was employed to acquire SVF values using the Google Street View (GSV) Image. The tool uses a deep learning AI algorithm developed by Liang et al. (2017, 2020) to extract the information from the GSV Image Database. The AI algorithm automates sky delineation using the convolutional neural network of SegNet, which classifies GSV pixels into sky, vegetation, and building in the form of hemispherical images (Liang et al., 2017, 2020). Based on these hemispherical images, the SVF is calculated according to the formulation below.

Table 2
Identified components and dominant variables (PCA analysis).

	Dimension	Proportion explained (%)	Dominant variable	Correlation
1	Chronic disease	46.82	Obesity, Diabetes, Asthma	0.3707
2	Heat exposures	12.85	LST, Ta_Max	0.6324
3	Social isolation	11.84	Living alone, Unemploy	0.3304
4	Street features	8.97	SVF, TVF	0.5085
5	AC-prevalence	6.21	Air conditioning central	0.5035

$$SVF = \frac{\sum_{i=0}^n w^*sky(i)}{\sum_{i=0}^n w} \tag{2}$$

$$f(i) = \begin{cases} 1, & \text{if } \alpha = 0 \text{ (pixel is sky)} \\ 0, & \text{if } \alpha > 0 \text{ (pixel is not sky)} \end{cases} \tag{3}$$

In these equations, n is the total number of pixels, w is a weight associated with each pixel, and $sky(i)$ is a binary function determined by whether the sky is visible at a pixel.

Employing a systematic sampling of observation spots along all the major streets of Houston, we obtained a sample location for every 100 m, which represent a good proxy of the pedestrian population density across accessible urban areas (City of Houston, 2020). A total of 11,200 sampling points were generated, evenly distributed over the city of Houston area (Fig. 3). SVF values were calculated for each sampling location and utilized in the COMFA models described above.

4. Results

4.1. Assessing heat vulnerability and street-level outdoor thermal comfort

The heat vulnerability and street-level outdoor thermal comfort (OTC) were assessed to explore their spatial patterns and identify their key determinants. The heat vulnerability index (HVI) score for 614 census tracts ranged from -9.3 to 19.3 , with a mean score of 0.01 , a slightly right-skewed distribution, and a median of -0.2 . The energy budget (EB) value, a street-level OTC measure, was between 126.7 W/m^2 and 159.1 W/m^2 . The mean value of the energy budget for all census tracts was 147.7 W/m^2 , falling under the ‘preferred to be cooler’ classification, suggesting that this figure was thermally hot and uncomfortable. According to the COMFA’s thermal threshold categorization (Kenny et al., 2009a, 2009b), approximately 30% and 70% of the census tracts exhibited values classified as ‘prefer to be much cooler (hot: over 150 W/m^2)’ and ‘prefer to be cooler (warm: $50 - 150 \text{ W/m}^2$)’ during the summer months, respectively.

To effectively identify the spatial patterns of heat vulnerability index and street-level outdoor thermal comfort, two types of maps – raw score and hot spot – were used (See Fig. 4). The left two maps of Fig. 4 indicate the spatial distribution of raw scores of heat vulnerability index and street-level outdoor thermal comfort values in Houston. The right two maps show clusters of hot and cold spots with significant local Moran’s I statistics at a p -value of 0.05 based on their scores and values. The red area is the cluster of the hot spot where the heat vulnerability and outdoor heat stress are higher than their averages; meanwhile, the blue area is the cold spot where they are lower than their averages. These maps demonstrate the uneven patterns of spatial distributions and variations of heat

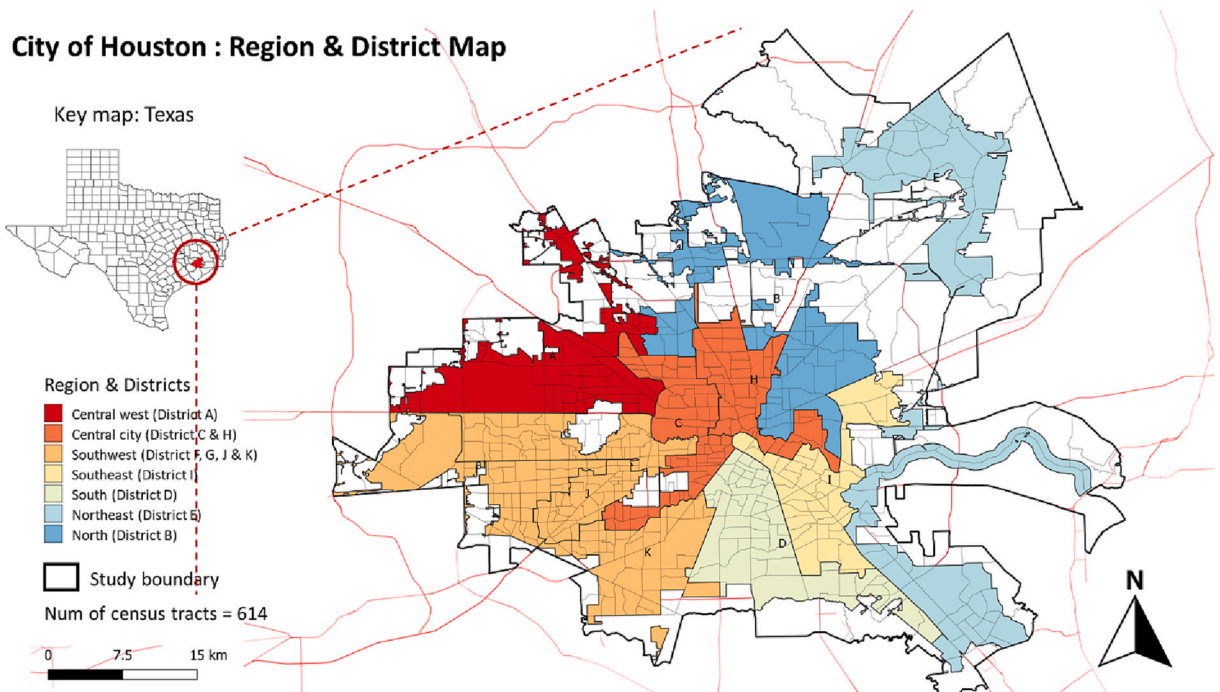


Fig. 1. City of Houston: Region and District Map.

** Note: District name - District A (Central west), District B (North), District C & H (Central city), District D (South), District E (Northeast), District I (Southeast), District F, G, J & K (Southwest).

vulnerability and outdoor thermal comfort, which presented the most thermally vulnerable areas where attention is warranted.

Regarding the hot and cold spots, heat vulnerability and outdoor thermal comfort showed different spatial patterns that partially overlapped with each other (See locator map of Fig. 1 and Fig. 4). For heat vulnerability, the census tracts located in the downtown bounded by Interstate 610 and the southeast area exhibited cold spots, or clusters of low heat vulnerability, whereas most sections of hot spots, or clusters of high heat vulnerability, were located in the north (District B), southeast (District I), and southeast section of District E, between Interstate 610 and Beltway 8 (See Fig. 1). Compared to heat vulnerability, outdoor thermal comfort showed a distinct pattern with mostly contiguous clusters of hot and cold spots. Most central west (District A) and southwest (Districts G & J) areas were classified as hot spots, while most northeast (District E) and southeast (District I) areas were classified as cold spots. When comparing the spatial distributions of the HVI and OTC, some overlaps existed in the north (District B) and southeast sections of District E. Notably, the downtown area is not vulnerable, exhibiting a cluster of cold spots indicating that is relatively thermally comfortable.

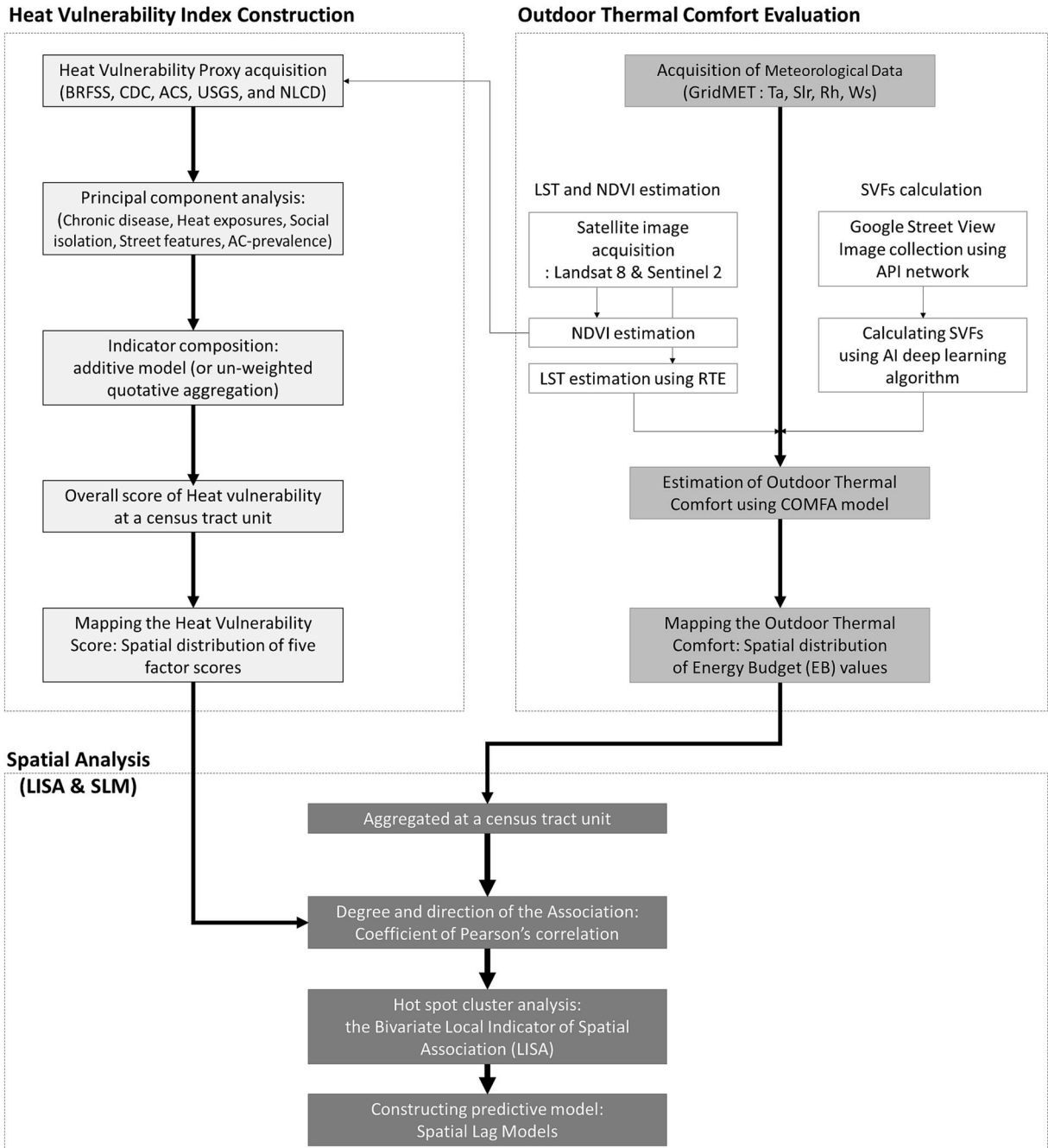


Fig. 2. Methodological steps taken in the study.

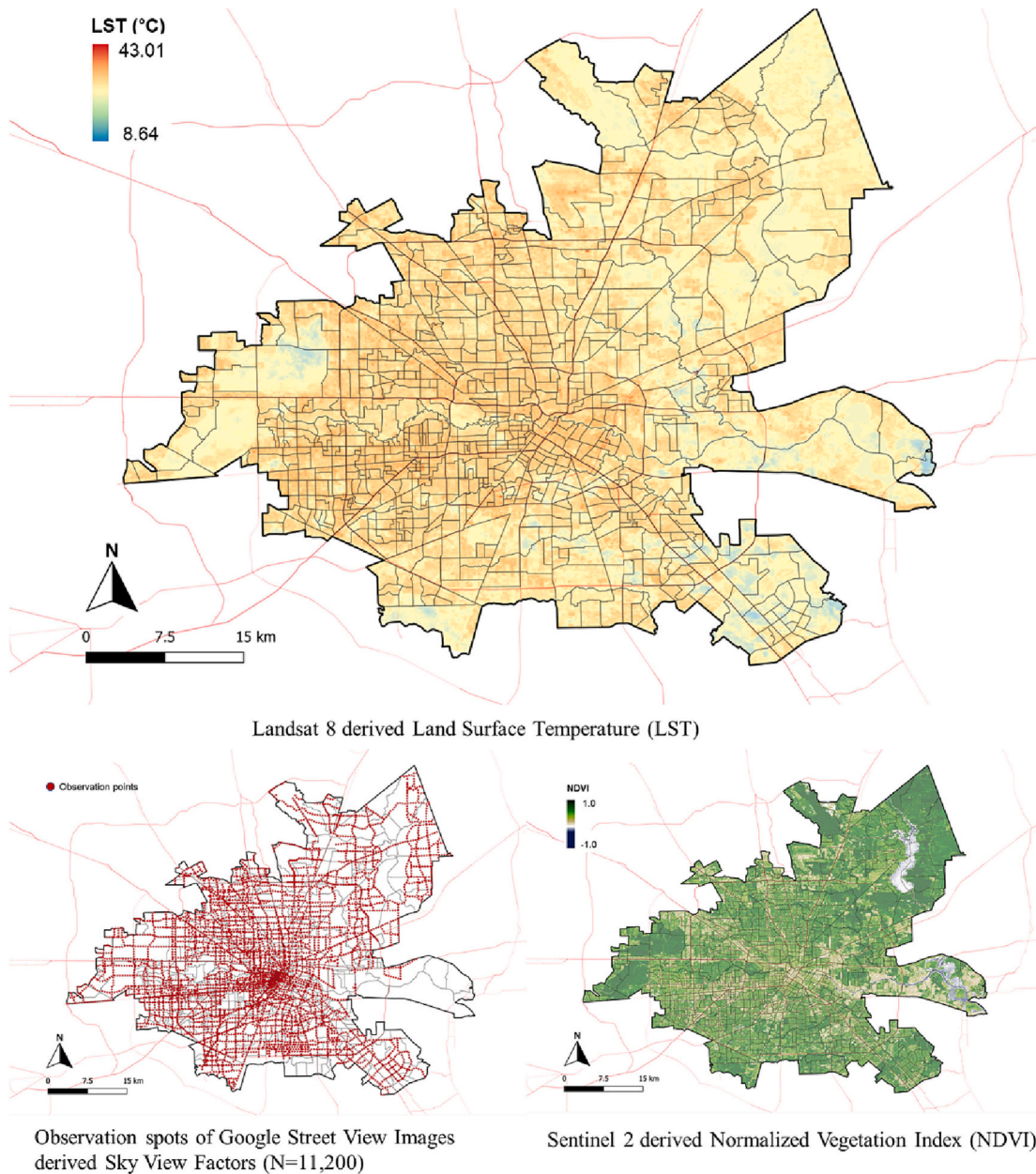


Fig. 3. Map of Landsurface temperture (LST), Normalized vegetation index (NDVI) and Sky view factors (SVFs).

Fig. 5 displays an in-depth examination of the five heat vulnerability components that were extracted to form the heat vulnerability index. These included chronic disease, heat exposure, social isolation, street features, and A/C prevalence, which were created by principal component analysis (PCA). The spatial distributions of each component are also presented in Appendix Fig. 1. The patterns of chronic disease, social isolation, and street features mostly coincided spatially with the overall patterns of HVI hot spots. Meanwhile, not surprisingly, hot spots of heat exposure and partial areas of street features largely overlapped with hot spots of street-level OTC located in the central west (District A) and southwest (District G & J). Detailed explanations of the distribution for individual heat vulnerability components are as follows.

The first component, chronic disease, represented pre-existing health conditions such as diabetes and obesity. Its vulnerability score was relatively higher in the north (District B), southeast (District I) and south (District D) areas of Houston, except for the central city (Districts C & H). The cold spots in the central city area stretched to the central west (District A) and southwest (Districts G & J). Hot and cold spots of chronic disease largely overlap with those of HVI. However, for the street-level OTC, only cold spots in the southeast section of District E intersected the chronic disease map.

The second component, heat exposure, referred to the meteorological thermal conditions combining ambient temperature (T_a) and

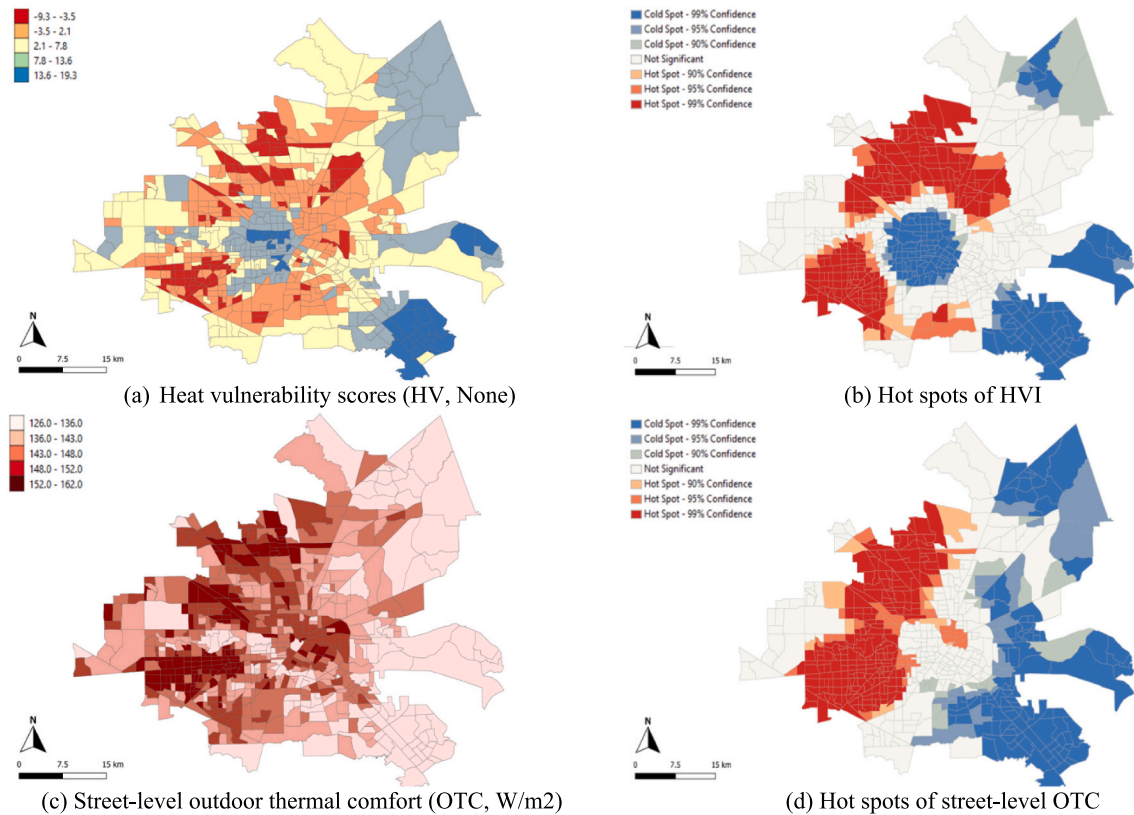


Fig. 4. Spatial distribution of heat vulnerability index scores (a) and street-level outdoor thermal comfort values (c) and their hot and cold spots (b and d) in Houston census tract ($N = 614$).

land surface temperature (LST). Hot spots were located in the central city, central west, and north areas of Houston. Cold spots were clustered in the south, southeast, and northeast areas. This is largely due to the land use patterns of city development and the amount of greenery concentrated in the west section of Houston. As expected, the spatial pattern of heat exposure was highly similar to that of street-level OTC.

The third component of street features was street-level built environment features that affect the amount of direct sunlight reaching the ground. Spatial patterns of street features largely matched with both HVI and street-level OTC. Cold spots were located in the central city (District C & H), which overlapped with HVI. Hot spots in the central west (District A) partially matched those of street-level OTC.

Lastly, the fourth and fifth components were social isolation and A/C prevalence. These were related to the ratio of individuals and older individuals living alone and with air conditioning systems, respectively. Only limited areas of social isolation hot spots in the central city (Districts C & H) and south (District E) areas spatially overlapped with those of HVI. The central city was identified with hot spots on the HVI map but with cold spots on the social isolation map. Regarding the A/C prevalence, cold spots in the city area only overlapped with those of HVI, with no intersections with either the hot or cold spots of street-level OTC.

Table 3 demonstrates the difference between hot and cold spots in the mean score of HVI and the value of street-level outdoor thermal conditions. For the HVI scores, the gaps between hot and cold spots were the largest for chronic disease at 4.0 and the least for social isolation at 0.2. For the outdoor thermal conditions, the differences between hot and cold spots in mean values of energy budget (EB), land surface temperature (LST), and ambient temperature (T_a) were 8.9 W/m², 2.7 °C, and 0.5 °C, respectively. Considering their difference of degree in standardized values, energy budget values ($|SD| = 1.8$) and surface temperature ($|SD| = 0.6$) showed relative higher spatial variations among the clusters compared to ambient temperature ($|SD| = 0.2$). This result illustrated that EB values and LST are superior indexes than T_a for heat vulnerability assessment given that they better reflect the spatial variation of heat vulnerability.

4.2. Association between heat vulnerability and outdoor thermal conditions

The coefficient of Pearson's correlation is reported in Table 4, which shows the degree and direction of the association. Energy budget (EB) values and HV scores had a strong and moderative positive relationship with heat exposure at 0.781 ($p = 0.1$) and 0.385 ($p = 0.1$) separately, which derived from the measurement of T_a and LST. On the other hand, street features and chronic disease showed a

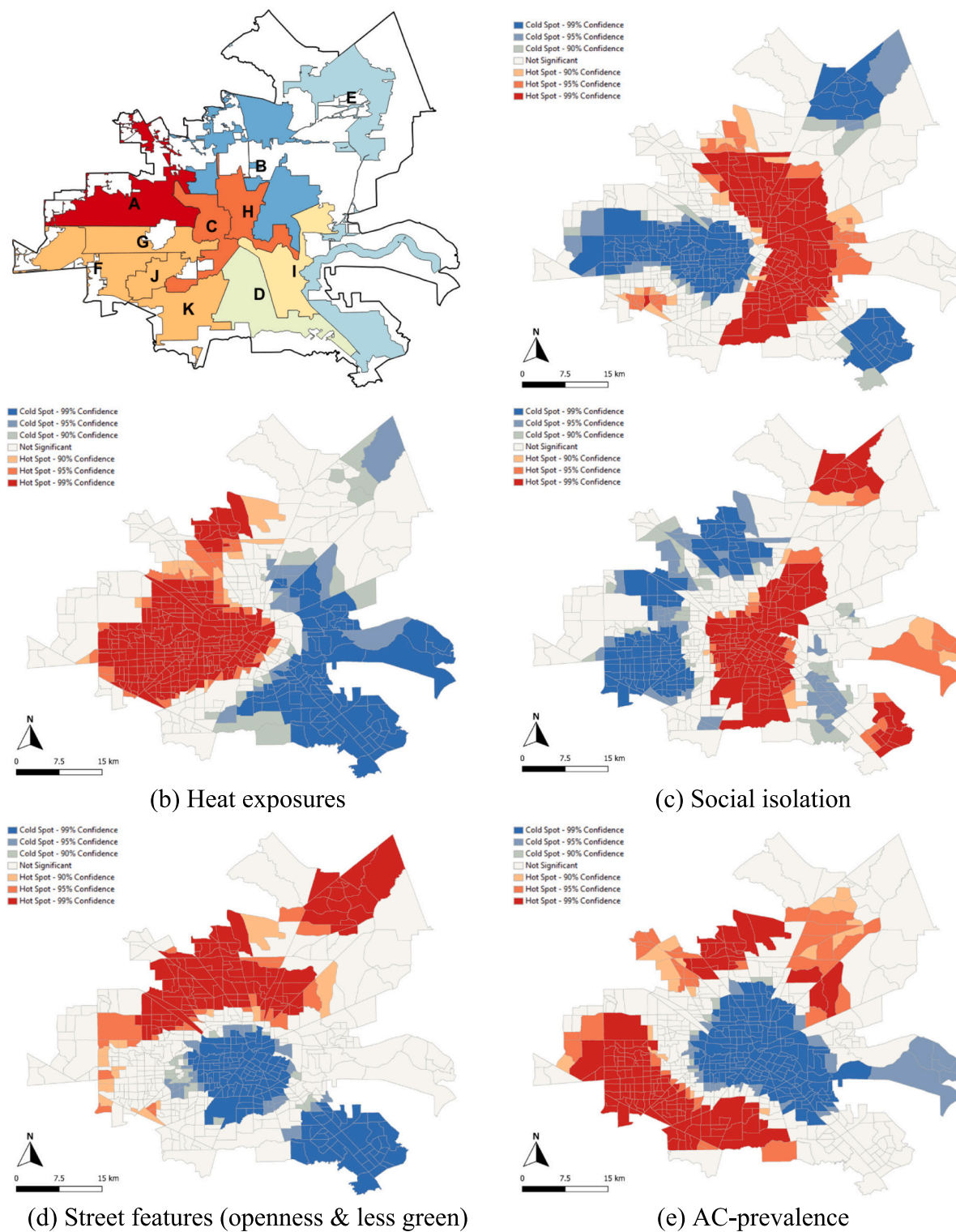
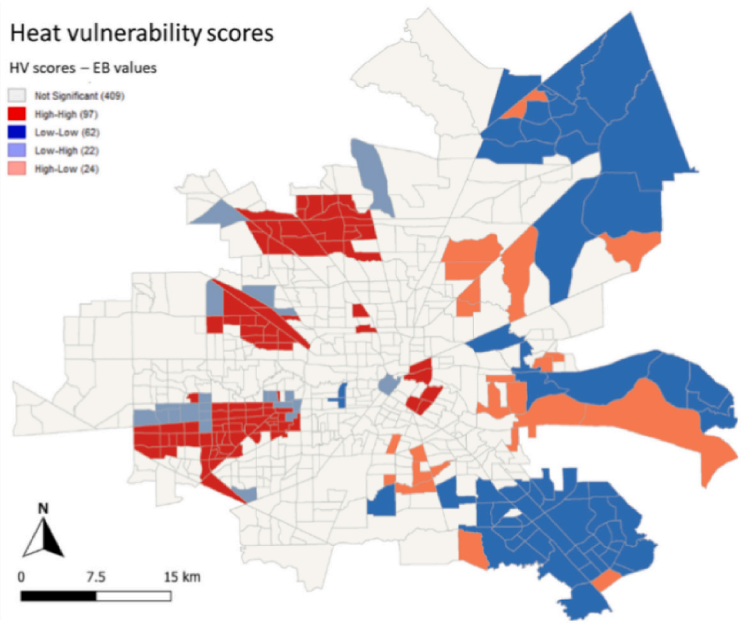
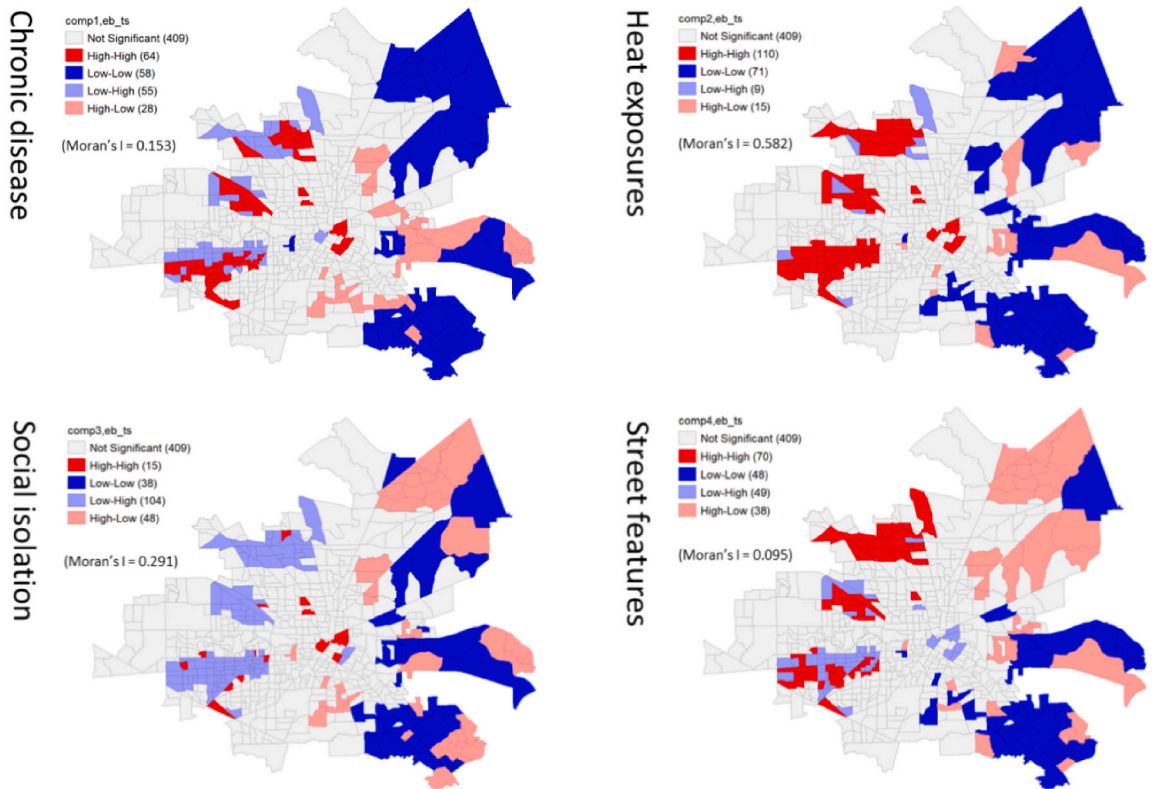


Fig. 5. Hot and cold spots of five identified components of heat vulnerability.

** Note: District name - District A (Central west), District B (North), District C & H (Central city), District D (South), District E (Northeast), District I (Southeast), District F, G, J & K (Southwest).

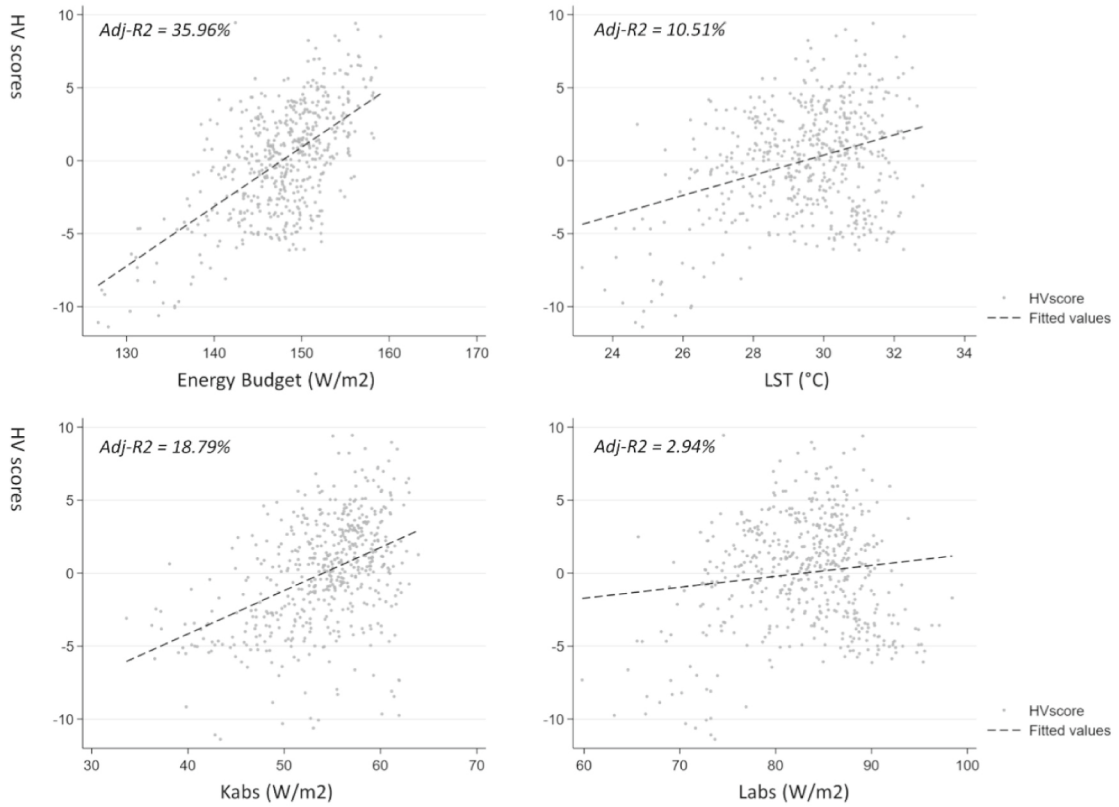


(a) LISA clusters between vulnerability scores and energy budget values (W/m^2)

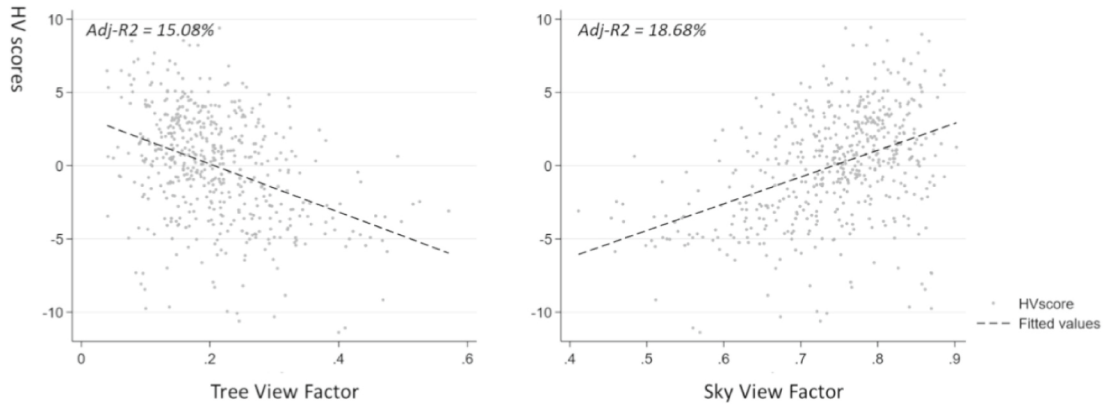


(b) LISA clusters between four vulnerability components and energy budget values (W/m^2)

Fig. 6. Bivariate LISA Cluster analysis between heat vulnerability and street-level outdoor thermal comfort of energy budget values (W/m^2).



(a) Relationship with street-level thermal conditions



(b) Relationship with street morphological features

Fig. 7. Binary linear-relationship of heat vulnerability index scores with street-level outdoor thermal conditions and physical street design features.

moderate negative ($r = 0.484, p = 0.1$) and a weak positive ($r = 0.200, p = 0.1$) relationship with EB values respectively. Not surprisingly, the correlation coefficient between energy budget values and A/C prevalence was not statistically significant ($r = 0.055$). Furthermore, the association between EB values and HVI scores was weak at 0.267 ($p = 0.1$), possibly due to the fact that HVI scores were largely affected by socio-economic variables, as shown in the high correlation coefficient of chronic disease at 0.735 ($p = 0.1$) and social isolation at 0.322 ($p = 0.1$).

Map (a) of Fig. 6 displays the Bivariate Local Indicator of Spatial Association (LISA) cluster map of HVI. The Bivariate LISA shows

Table 3

Difference between hot and cold spots in heat vulnerability index scores ($N = 124$) and outdoor thermal condition values ($N = 127$).

	Cold spot			Hot spot			Δ	Δ Diff (Hot-Cold) SD
	N	Mean	SD	N	Mean	SD		
Heat vulnerability components								
Chronic disease	124	-2.1	1.9	184	1.9	1.7	4.0	-0.2
Heat exposures	124	-0.4	1.9	184	0.1	1.0	0.4	-0.9
Social isolation	124	0.3	1.1	184	0.0	1.5	0.2	0.4
Street features	124	-0.7	1.1	184	0.4	0.9	1.1	-0.2
AC-prevalence	124	-0.4	0.6	184	0.1	1.1	0.5	0.5
Outdoor thermal conditions								
EB (W/m ²)	127	141.8	5.6	247	150.7	3.8	8.9	-1.8
LST (°C)	127	27.6	1.7	247	30.3	1.1	2.7	-0.6
Ta (°C)	127	34.0	0.3	247	34.5	0.1	0.5	-0.2

Table 4

Pearson’s correlation for heat vulnerability index scores, its components and street-level outdoor thermal comfort values in Houston census tract ($N = 614$).

	(1)	(2)	(3)	(4)	(5)	(6)	(7)
(1) EB value	1.000						
(2) HV score	0.267*** (0.000)	1.000					
(3) Chronic disease	0.200*** (0.000)	0.735*** (0.000)	1.000				
(4) Heat exposures	0.781*** (0.000)	0.385*** (0.000)	0.000 (1.000)	1.000			
(5) Street features	-0.484*** (0.000)	0.370*** (0.000)	0.000 (1.000)	0.000 (1.000)	1.000		
(6) Social Isolation	-0.049 (0.268)	0.322*** (0.000)	0.000 (1.000)	0.000 (1.000)	0.000 (1.000)	1.000	
(7) AC-prevalence	0.055 (0.215)	0.268*** (0.000)	0.000 (1.000)	0.000 (1.000)	0.000 (1.000)	0.000 (1.000)	1.000

P-value in parentheses | *** $p < 0.001$, ** $p < 0.01$, * $p < 0.05$.

the locations of similar high and low values of HVI scores and street-level OTC while testing for neighboring polygons. With the significance at 0.05, the areas highlighted in red are the clusters of hot spots, where high HVI values coexisted with high energy budget values in neighboring census tracts. The areas highlighted in blue are the clusters of cold spots, where lower HVI values were observed adjacent to lower energy budget values. According to the LISA map, part of the southeast, central west, and north section fell into the hot spots with higher HVI scores and higher energy budget values. Conversely, the far east section, such as northeast and southeast close to the boundary of Houston city, was classified as having cold spots with lower HVI scores and lower energy budget values. In these cluster areas, the HVI scores were relatively sensitive to street-level OTC conditions; thus, their relationship would be more substantial than in other sections of Houston.

The bivariate LISA maps between the four components of HVI (i.e., chronic disease, heat exposure, social isolation, and street features) and street-level OTC were further mapped using local Moran’s I value to explore their Hot and Cold spots (Map (b) of Fig. 6). The A/C prevalence component was excluded, as its Pearson correlation with energy budget values was not significant (Table 4). As the global Moran’s I value indicated, all the components except for social isolation were spatially correlated with energy budget values. Heat exposure had the highest global Moran’s I value at 0.582, and then street features at 0.291 and chronic disease at 0.153 were followed, whose order of strength association was similar to the Pearson’s correlation results displayed in Table 4.

We have further explored the street-level factors of thermal conditions and physical street design influencing the HVI scores (Fig. 7). The factors of thermal conditions include energy budget (EB), land surface temperature (LST), absorbed solar radiation of people (Kabs), and absorbed terrestrial radiation of people (Labs).

Binary relationships between HVI scores and factors of street-level thermal conditions are presented in the scatter plot (a) of Fig. 7. According to the binary plots, all four factors of thermal conditions had positive relationships with HVI scores. Looking at individual variables, energy budget values had a positive relationship with HVI and the highest explanatory power in describing the variations of HVI, with adj-r² values of around 36%. Meanwhile, the explanatory powers of LST and Kabs were moderate at 10.51% and 18.79%, respectively. Labs had the least adj-r² of 2.94%. These plots implied that the human outdoor thermal comfort index is a superior indicator of heat-related risks compared to single meteorological factors such as LST, Kabs, and Labs.

Two plots (b) of Fig. 7 illustrate the relationships between HVI scores and physical street design features. Tree View Factors (TVFs) and Sky View Factors (SVFs) are dominant built environmental indicators that determine the outdoor thermal comfort of people walking at the street scales. They had moderate explanatory power ranging between 15.0% and 18.6% in predicting the variation of

HVI scores, but their directions of impact were opposite to each other. As TVFs increased, HVI scores declined because less solar radiation reached the ground. Meanwhile, SVFs elevated the HVI scores, as larger openness of streets with less greenery results in receiving more sunshine, leading to increased LST and OTC.

4.3. Impact of heat vulnerability and outdoor thermal comfort on heat-related illnesses

Table 5 displays heat vulnerability components' impact on the number of emergency department (ED) visits by street-level outdoor thermal comfort. The five components of heat vulnerability were significantly associated with the number of ED visits but yielded different coefficients in the high versus low clusters of energy budget (EB) values.

The predictive performance of our suggested model for the number of ED visits was approximately 25% on average, but significantly relies on EB values. The area with high EB values (over 200 W/m²) had a relatively higher explanatory power (adj-R²) of 29.0% for the OLS model and 37.9% for the SLM model (Appendix Table 3). For the low (vs. high) EB value areas, both models' explanatory power was much lower at approximately 8.7%. These results illustrated that our heat vulnerability index had a high explanatory power when assessing the areas that suffered from higher levels of outdoor human thermal stress. We thus concluded that SLM specification is the preferred approach. When the spatial autocorrelation, and specifically the spillover effect, was accounted for by the SLM model, the explanatory power considerably increased by around 8.0% compared to OLS model. Furthermore, the LM test indicated SLM specification is preferred, and AIC/BIC tests showed the parsimonious values with SLM. Direct and indirect estimations of SLM were presented in Appendix Table 4, 5 and 6.

Regarding the effects of the five individual heat vulnerability components on ED visits, their degrees of impact were statistical significance across the appropriate models. In the SLM model specification, for all levels of EB value areas, the variables of chronic disease and hot spots were significant statistically at a *p*-value of 0.05. We assumed that this is mainly due to the binary variable of hot and cold spots introduced in the model. For the high-EB value areas, heat exposure and street features have a positive and significant relationship with the number of ED visits. Meanwhile, none of the variables were statistically significant in low-EB value areas. This means that chronic disease was the most influential determinant of heat vulnerability for all levels of EB value, while the effects of other variables can vary significantly depending on the EB values and the analytical models adopted.

5. Discussion

The results of this study highlight the relationship between heat vulnerability, outdoor thermal comfort, and heat-related disease in the city of Houston. We identified five heat vulnerability components – chronic disease, heat exposure, social isolation, street features, and A/C prevalence – while exploring the clusters of vulnerability hot spots. It was found that heat vulnerability index scores have a

Table 5
SLM specification: Impact of heat vulnerability components on number of ED visits by street-level outdoor thermal comfort.

	All levels-EB values (All spots)	High-EB values (Hot spot)	Low-EB values (Cold spot)
Chronic disease	0.617** (0.188)	0.359 (0.286)	0.563 (0.393)
Heat exposures (Meteorological status)	0.360 (0.472)	2.358** (0.839)	-0.159 (0.793)
Social isolation	-0.384 (0.379)	-0.650 (0.592)	0.015 (0.760)
Street features (openness & less green)	0.738 (0.423)	1.760* (0.736)	-0.350 (0.702)
AC-prevalence	0.934 (0.503)	0.263 (0.794)	-0.120 (1.106)
Hot & Cold spot			
- Hot spot	-2.581* (1.243)		
- Cold spot	-0.467 (1.477)		
_Cons	8.778*** (1.426)	3.861* (1.528)	38.945*** (2.406)
Var (ED visit)	100.044*** (6.483)	0.828*** (0.038)	0.798*** (0.057)
N	515	247	127
Adj. R ² & Pseudo R ²	0.231	0.379	0.087
Mean VIF	-	-	-
Global Moran I's	-	-	-
Wald test	0.805	0.827	0.798
Log-likelihood	-1959.228	-920.553	-484.60
AIC/BIC test	3938.45/3980.89	1857.10/1885.18	985.21/1007.97

Standard errors in parentheses | *** *p* < 0.001, ** *p* < 0.01, * *p* < 0.05.

Num of ED visits = inbound + outbound patients.

strong positive bivariate relationship with street-level outdoor thermal conditions of EB and Kabs and with physical street design features of TVFs. Our multivariate models showed that the greater the heat vulnerability score and street-level outdoor thermal comfort were, the better the models performed in explaining the variation of the number of ED visits, representing a unique finding of this study.

Our hotspot cluster analysis (LISA) identified slightly different spatial patterns between the heat exposure component of the heat vulnerability index (HVI) and street-level outdoor thermal comfort (OTC) (See Fig. 6). The clusters of hot and cold spots only partially overlapped between the two, indicating a difference in locating the high thermal areas according to the heat stress evaluation method and indicator selection. Two possible explanations can be proposed for this phenomenon. First, street-level OTC only includes public spaces such as streets, parks, and plazas that residents can access or use in our street-level thermal comfort evaluation. Therefore, forests, rivers, seacoasts, meadows, and building rooftops are excluded from the assessment, as accessible routes did not exist in these areas and therefore Google Street View images were unavailable. Therefore, our analysis results are closer to the actual heat exposure level of urban residents because only outdoor public spaces urban residents use were assessed.

Second, street-level OTC measures the physiological thermal comfort that is close to the actual thermal sensation of urban residents, which meteorological factors cannot easily capture. To calculate the HVI's heat exposure component, single meteorological indicators of Ta and LST were utilized. Meanwhile, energy budget values (W/m²) were estimated using multiple sets of meteorological parameters (Ta, LST, Rh, and Slr) while considering principles of the human energy budget model. Specifically, during the hot summer daytime, high temperatures combined with higher relative humidity and stronger wind speed are likely to cause higher thermal stress than people may actually feel according to the recorded ambient temperature, which can be captured by outdoor thermal comfort indexes (Kim and Brown, 2022). Moreover, the COMFA model considers short- and long-wave solar radiation determined by street morphological features using SVFs parameters, which allows us to estimate microclimate conditions at the street scale required for the calculation of human outdoor thermal comfort.

Our analysis results indicated that chronic disease and heat exposure components strongly impacted HVI while showing high Pearson's correlation coefficient and Local Moran's I statistics (See Table 4 and Fig. 6). This result implies that these are major determinants of HVI scores with relatively stronger influences. These findings are similar to past study results illustrating that pre-existing health conditions, specifically diabetes and stroke, as well as higher Ta and LST, are significant contributors to heat-related disease and vulnerability index scores (Prudent et al., 2016; Christenson et al., 2017). Meanwhile, A/C prevalence is not significant in our findings, in contrast to similar past studies (Reid et al., 2012; Sharma et al., 2018). We assume this discrepancy is mainly due to the high thermal threshold of people living in Houston – Texans who are familiar with hot summer weather conditions in this humid subtropical climate. Another possible reason is the higher rates of A/C prevalence than in other US regions because Texas law or lease agreements may require landlords to protect their tenants against extreme temperatures or repair a faulty A/C unit (Section 92.052 of the Texas Property Code).

Our multivariate model illustrated that the relationship between heat vulnerability and ED visits depends on street-level outdoor thermal comfort (Table 5). In the clusters of census tracts with higher energy budget values, our model had higher performance, whereas thermal cold spots had relatively lower explanatory power. Specifically, in areas with higher energy budget values and a higher HVI score, our model showed improved predictive power in explaining the variation in the number of ED visits. These findings imply that outdoor thermal comfort conditions are significantly associated with the relationship between HVI scores and the frequency of heat-related diseases, showing the potential applicability of the energy budget model-based outdoor thermal comfort index to heat vulnerability assessment. Therefore, future studies should develop methodology or techniques to incorporate the outdoor thermal comfort index into the vulnerability assessment.

Despite our study's novelty, one notable limitation exists. The temporal mismatch of some datasets may have affected the model estimations. Most of the datasets used were collected from 2018 to 2020. However, due to the data availability, the satellite imageries (Landsat8 and Sentinel) used in this study were collected for only three days in the summer months of 2019 and 2020, which were not precisely corresponding to collection periods of the socio-economic, built environment, and pre-existing health condition variables. This inconstant may decrease the explanatory power of our suggested models.

6. Conclusion

This study explores the interrelationship among outdoor thermal comfort (OTC), the heat vulnerability index (HVI), and heat-related illnesses in Houston. The results indicated that our models have better explanatory power over the number of emergency department (ED) visits when there are higher HVI scores and more comfortable street-level OTC. A positive relationship was found between HVI scores and EB values, with an adj-r² of approximately 36%. Chronic disease and heat exposure significantly impacted the HVI, while tree and sky view were key determinants of the EB values.

Our study addresses gaps in the current understanding of heat-related risks by (1) assessing spatially explicit heat exposure factors at the street level and (2) taking into account human physiological responses to thermal stress. This provides a new approach to evaluating heat vulnerability and exposure at the human scale, which offers scholars, planners, and policymakers effective evaluation tools and guidelines to address the increasing risk of urban heat islands and heat-related diseases. Moreover, in the era of climate change, this study also supports the Sustainable Development Goals (SDGs) by promoting the equitable distribution of resources. This can be accomplished through the suggested heat vulnerability assessment in this study, which focuses on people and socio-economic factors aimed at mitigating the climate change risk.

Future studies should aim to obtain temporally matched datasets to improve the explanatory power of models. As discussed previously, the temporal mismatch of some datasets may have affected the model estimations in this study. Therefore, future studies

should match the collection periods of satellite imagery with those of the socio-economic, built environment, and pre-existing health condition variables. Secondly, further investigation is necessary to explore the relationship between heat-related illnesses and outdoor thermal comfort at different times of day and seasons. This is necessary for the effective evaluation of urban heat mitigation strategies. Lastly, future studies should investigate the predictive performance of empirical models for heat-related diseases using various heat indexes for practical applications in the real world.

Funding acknowledgement

The authors disclosed receipt of the following financial support for the research, authorship, and publication of this article: This work was financially supported by the Center for Health & Nature Research Innovation Fund and the Gulf Research Program Early-Career Research Fellowship of the National Academies of Sciences, Engineering, and Medicine (2000012329).

CRedit authorship contribution statement

YouJoung Kim: Conceptualization, Methodology, Software, Formal analysis, Investigation, Data curation, Writing – original draft, Writing – review & editing, Visualization, Supervision. **Dongying Li:** Investigation, Data curation, Writing – original draft, Writing – review & editing, Project administration, Funding acquisition. **Yangyang Xu:** Investigation, Data curation, Writing – original draft. **Yue Zhang:** Data curation, Writing – original draft. **Xiaoyu Li:** Data curation, Writing – original draft. **Lexi Muhlenforth:** Data curation, Writing – original draft. **Shengliang Xue:** Writing – original draft. **Robert Brown:** Investigation, Project administration, Funding acquisition.

Declaration of Competing Interest

The authors declare the following financial interests/personal relationships which may be considered as potential competing interests.

The authors disclosed receipt of the following financial support for the research, authorship, and publication of this article: This work was financially supported by the Center for Health & Nature Research Innovation Fund and the Gulf Research Program Early-Career Research Fellowship of the National Academies of Sciences, Engineering, and Medicine (2000012329).

Data availability

The authors do not have permission to share data.

Appendix A. Appendix

Appendix Table 1

Variables used in the literature to represent human heat exposure/stress.

	Climate factors	Variables	Example studies
1	Land surface temperature	Land surface temperature	Aminipouri et al., 2016; Johnson et al., 2012; Morabito et al., 2015
2	Air temperature	Day/night temperature Heatwave days	Zhang et al., 2019 Tran et al., 2020; Kim et al., 2017
3	Solar radiation	Street incoming solar radiation Roof incoming solar radiation	Maragno et al., 2020 Maragno et al., 2020
4	Thermal index	WBGT Humidex	Zheng et al., 2020 Aminipouri et al., 2016; Krstic et al., 2017

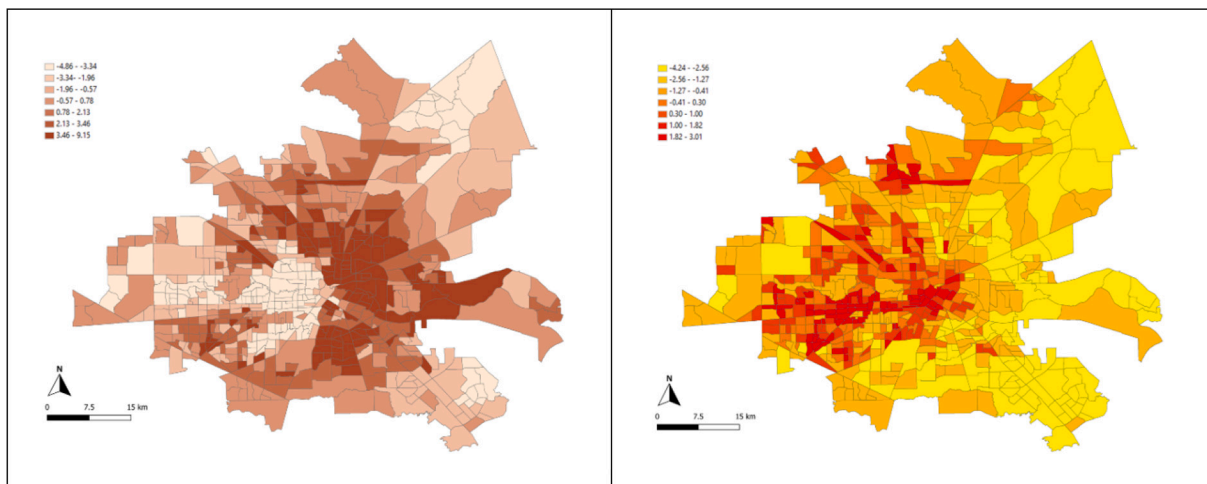
Appendix Eq. (1) Radiative Transfer Equation (RTE)

This study adopts the Radiative Transfer Equation (RTE) method to calculate Landsat 8 derived -Land Surface Temperature (LST). LST retrieval through RTE involves modeling the radiative transfer processes within the Earth’s atmosphere and the interaction between the surface and the atmosphere. It involves atmospheric correction, applying the Split-Window algorithm, and calibration/validation to improve accuracy.

The Radiative Transfer Equation (RTE) is a complex mathematical equation that describes the radiative energy transfer in the atmosphere. It is typically represented as:

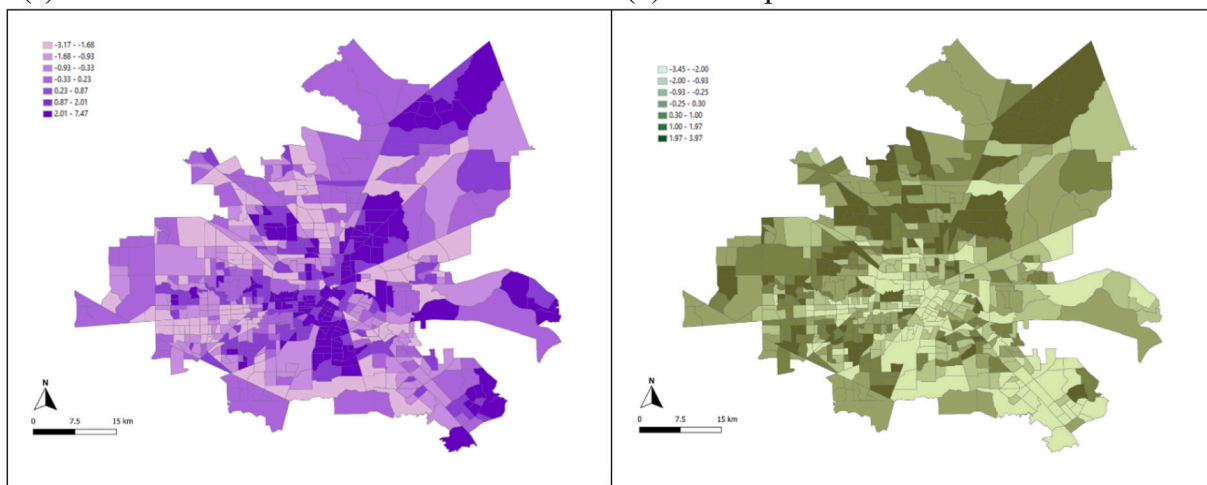
$$I(\lambda) = T(\lambda) * \left[E_{-s}(\lambda) * \tau_{-s}(\lambda) * \rho_{-s}(\lambda) + \int (E_{-a}(\lambda) * \tau_{-a}(\lambda) * \rho_{-a}(\lambda) * T_{-a}(\lambda) * exp.(- \tau(\lambda))) * d\tau \right] \tag{1}$$

In this equation, I(λ) represents the measured radiance at a specific wavelength (λ), T(λ) is the atmospheric transmittance, E_s(λ) and E_a(λ) are the surface and atmospheric emittances respectively, τ_s(λ) and τ_a(λ) are the surface and atmospheric transmittances, ρ_s(λ) and ρ_a(λ) are the surface and atmospheric reflectances, T_a(λ) is the atmospheric temperature, τ(λ) is the optical thickness, and the integral term represents the summation of radiative contributions from different atmospheric layers.



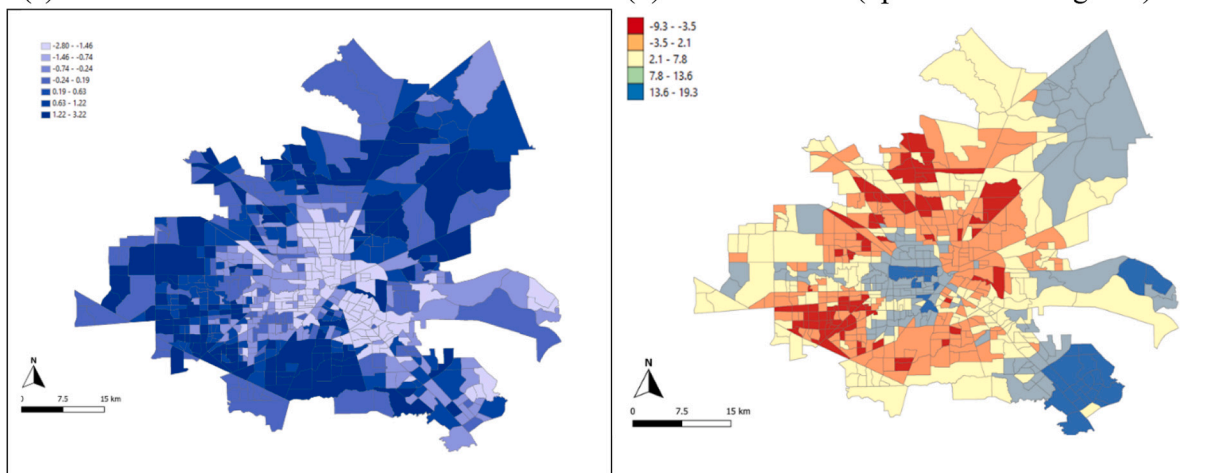
(a) Chronic disease

(b) Heat exposures



(c) Social isolation

(d) Street features (openness & less green)



(e) A/C prevalence

(f) Heat vulnerability score

Appendix Fig. 1. Five Identified components of heat vulnerability.

Appendix Table 2
Initial variables selected based on the literature review of heat vulnerability assessment*.

HVI Component	Classification	Sub-classification	Variables	A	B	C	D	E	F	G	H	I	J	K	L	M	
Exposure	environ hazard	climate & weather	Air temperture (Dbt / Wbt / Extrmer Heat wave / Modeled)		0	0		0					0			0	0
Exposure	environ hazard	climate & weather	Land Surface Temp (LST; night/day)			0	0		0	0	0						
Exposure	environ hazard	air quality	Air quality, PM2.5														0
Exposure	environ hazard	air quality	Air quality ozone														0
Exposure	built environment	greenry & vegetation	% Imperviousness surface			0			0								
Exposure	built environment	greenry & vegetation	% Roof cover material (green & gray)		0												
Exposure	built environment	housing density	Housing density		0				0								
Exposure	built environment	urban form	Urban Canyon Ratio (HW ratio)														
Exposure	built environment	urban form	Avg building height														
Exposure	built environment	urban form	Sky View Factor (BVs & TVFs)														
Exposure	built environment	urban form	Street orientation														
Exposure	built environment	urban form	% Building cover ratio (BCR)														
Exposure	built environment	urban form	% Floor-area ratio (FAR)														
Exposure	built environment	greenry & vegetation	% Nongreen space / nearby green space (std dev)	0			0					0	0	0	0	0	0
Exposure	built environment	greenry & vegetation	Normalized difference built-up index (NDBI)								0						
Exposure	built environment	greenry & vegetation	Normalized difference vegetation index (NDVI)				0		0	0	0					0	
Exposure	built environment	landuse & landcover	Vegetation cover			0	0	0								0	
Exposure	built environment	landuse & landcover	Developed land cover					0								0	
Exposure	built environment	landuse & landcover	Material index (light materials)					0		0							
Sensitivity	socioeconomic	poverty	% Residents below the poverty line	0	0		0	0	0		0	0	0	0	0	0	0
Sensitivity	socioeconomic	employment	% Unemployment			0				0							
Sensitivity	socioeconomic	education	% Education (without highschool diploma)	0	0	0		0		0	0	0		0	0	0	0
Sensitivity	socioeconomic	income	% Households income / Rental housing cost		0			0	0	0	0						
Sensitivity	socioeconomic	gender	% Females head of household			0					0						
Sensitivity	socioeconomic	poverty	Housing value (median)						0								
Sensitivity	demographic	age	% Population age 65 or older	0	0	0	0	0	0	0	0	0	0	0	0	0	0
Sensitivity	demographic	age	% Young population below 5		0	0		0		0							0
Sensitivity	demographic	population density	Population density			0		0									0
Sensitivity	demographic	race & ethnicity	% Race (Non-white / Non-African)		0	0	0	0	0		0	0	0	0	0	0	0
Sensitivity	social isolation	minority	% People living alone (all / elderly pop)	0	0	0	0		0			0	0	0	0	0	0
Sensitivity	social isolation	language isolation	% Linguistically isolated households	0	0				0				0				
Sensitivity	social isolation	minority	% Households with seven or more residents						0								
Sensitivity	social isolation	minority	% Single family unit / detached homes		0				0								
Sensitivity	health condition	pre-existing medical condition	% Diagnosed with diabetes (or others)	0	0							0	0	0	0	0	0

(continued on next page)

Appendix Table 2 (continued)

HVI Component	Classification	Sub-classification	Variables	A	B	C	D	E	F	G	H	I	J	K	L	M
Sensitivity	health condition	pre-existing medical condition	% People with disabilities						O							
Sensitivity	health condition	pre-existing medical condition	% People with mental health		O	O										
Adaptive capacity	home amenity	air conditioning prevalence	% Homes with no air conditioning / central air conditioning		O	O	O	O				O	O		O	
Adaptive capacity	neighborhood stability	building & housing quality	% Residents changed households						O							
Adaptive capacity	neighborhood stability	building & housing quality	% Vacant households						O							
Adaptive capacity	neighborhood stability	building & housing quality	% Year house built (median)						O							
Adaptive capacity	healthcare access	medical resources	Nursing home bed count													O
Adaptive capacity	healthcare access	medical resources	Access to medical services (Proximity to hospitals)							O						
Adaptive capacity	healthcare access	healthcare system	Access to communication technologies							O						
Adaptive capacity	healthcare access	medical resources	Health insurance coverage	O												
Adaptive capacity	mobility	transportation	Households without vehicle				O									O
Adaptive capacity	accessibility to resources	Proximity to green space	Proximity to water bodies													
Adaptive capacity	accessibility to resources	Proximity to green space	Proximity to cool shelters				O						O			
Adaptive capacity	accessibility to resources	Proximity to green space	Proximity to public transportation/major road													

* A - Aubrecht and Ozceylan (2013); B - Sharma et al. (2018); C - Prudent et al. (2016); D - Harlan et al. (2013); E - Harlan et al. (2006); F - Uejio et al. (2011); G - Inostroza et al. (2016); H - Johnson et al. (2012); I - Reid et al. (2012); J - Bradford et al. (2015); K - Maier et al. (2014); L - Chuang and Gober (2015); M - Christenson et al. (2017).

Appendix Table 3

SLM specification (direct/indirect/total coefficient): All level – Energy Budget.***

	Delta-Method		z	P > z	[95% conf. interval]	
	dy/dx	std.err.				
Direct						
comp1	0.76	0.23	3.39	0.00	0.32	1.21
comp2	0.45	0.58	0.76	0.45	-0.70	1.59
comp3	-0.48	0.47	-1.02	0.31	-1.39	0.44
comp4	0.91	0.52	1.76	0.08	-0.10	1.93
comp5	1.16	0.62	1.87	0.06	-0.06	2.37
hot & cold						
hot spot	-3.20	1.54	-2.08	0.04	-6.21	-0.19
cold spot	-0.58	1.83	-0.32	0.75	-4.17	3.01
Indirect						
comp1	2.40	0.70	3.42	0.00	1.02	3.78
comp2	1.40	1.85	0.75	0.45	-2.23	5.03
comp3	-1.49	1.46	-1.02	0.31	-4.36	1.38
comp4	2.87	1.60	1.79	0.07	-0.27	6.01
comp5	3.63	1.98	1.84	0.07	-0.24	7.51
hot & cold						
hot spot	-10.04	5.06	-1.98	0.05	-19.96	-0.12
cold spot	-1.82	5.79	-0.31	0.75	-13.16	9.52
total						
comp1	3.17	0.90	3.51	0.00	1.40	4.93
comp2	1.85	2.44	0.76	0.45	-2.93	6.62
comp3	-1.97	1.93	-1.02	0.31	-5.75	1.81
comp4	3.78	2.11	1.80	0.07	-0.34	7.91
comp5	4.79	2.58	1.86	0.06	-0.26	9.84
hot & cold						
hot spot	-13.23	6.53	-2.03	0.04	-26.04	-0.43
cold spot	-2.40	7.62	-0.31	0.75	-17.32	12.53

*** Comp1(Chronic disease), comp2 (Heat exposures) comp3(Social isolation) comp4(Street features) comp5(AC-prevalence).

Appendix Table 4

SLM specification (direct/indirect/total coefficient): High level – Energy Budget***.

	Delta-Method		z	P > z	[95% conf.interval]	
	dy/dx	std.err.				
Direct						
comp1	0.47	0.37	1.28	0.20	-0.25	1.19
comp2	3.07	1.07	2.86	0.00	0.97	5.17
comp3	-0.84	0.77	-1.10	0.27	-2.35	0.66
comp4	2.29	0.93	2.47	0.01	0.47	4.10
comp5	0.34	1.03	0.33	0.74	-1.68	2.36
Indirect						
comp1	1.62	1.24	1.31	0.19	-0.80	4.05
comp2	10.64	4.29	2.48	0.01	2.23	19.04
comp3	-2.93	2.71	-1.08	0.28	-8.25	2.39
comp4	7.94	3.31	2.40	0.02	1.45	14.43
comp5	1.19	3.54	0.33	0.74	-5.75	8.12
Total						
comp1	2.09	1.59	1.31	0.19	-1.03	5.21
comp2	13.70	5.21	2.63	0.01	3.48	23.92
comp3	-3.78	3.46	-1.09	0.28	-10.57	3.01
comp4	10.23	4.13	2.48	0.01	2.14	18.32
comp5	1.53	4.57	0.33	0.74	-7.42	10.48

*** Comp1(Chronic disease), comp2 (Heat exposures) comp3(Social isolation) comp4(Street features) comp5(AC-prevalence).

Appendix Table 5

SLM specification (direct/indirect/total coefficient): Low level – Energy Budget***.

	Delta-Method		z	P > z	[95% conf. interval]	
	dy/dx	std.err.				
Direct						
comp1	0.73	0.50	1.47	0.14	-0.24	1.71
comp2	-0.21	1.03	-0.20	0.84	-2.22	1.81
comp3	0.02	0.99	0.02	0.99	-1.92	1.96
comp4	-0.46	0.92	-0.49	0.62	-2.26	1.35
comp5	-0.16	1.44	-0.11	0.91	-2.98	2.66
Indirect						
comp1	2.05	1.39	1.48	0.14	-0.66	4.77
comp2	-0.58	2.88	-0.20	0.84	-6.22	5.06
comp3	0.05	2.78	0.02	0.99	-5.39	5.49
comp4	-1.28	2.70	-0.47	0.64	-6.58	4.02
comp5	-0.44	4.05	-0.11	0.91	-8.37	7.49
Total						
comp1	2.79	1.85	1.51	0.13	-0.84	6.41
comp2	-0.78	3.90	-0.20	0.84	-8.44	6.87
comp3	0.07	3.76	0.02	0.99	-7.31	7.45
comp4	-1.73	3.62	-0.48	0.63	-8.82	5.36
comp5	-0.59	5.48	-0.11	0.91	-11.34	10.16

*** Comp1(Chronic disease), comp2 (Heat exposures) comp3(Social isolation) comp4(Street features) comp5(AC-prevalence).

References

- Abatzoglou, J T, 2013. Development of gridded surface meteorological data for ecological applications and modelling. *Int. J. Climatol.* 33, 121–131.
- Aminipouri, M., Knudby, A., Ho, H.C., 2016. Using multiple disparate data sources to map heat vulnerability: Vancouver case study. *Can. Geogr.* 60 (3), 356–368.
- Anderson, G.B., Bell, M.L., Peng, R.D., 2013. Methods to calculate the heat index as an exposure metric in environmental health research. *Environ. Health Perspect.* 121 (10), 1111–1119.
- Anguelov, D., Dulong, C., Filip, D., Frueh, C., Lafon, S., Lyon, R., Ogale, A., Vincent, L., Weaver, J., 2010. Google street view: capturing the world at street level. *Computer* 43 (6), 32–38.
- Anselin, Luc, 2002. Under the hood: issues in the specification and interpretation of spatial regression models. *Agric. Econ.* 27 (3), 247–267.
- Aubrecht, C., Ozceylan, D., 2013. Identification of heat risk patterns in the U.S. National Capital Region by integrating heat stress and related vulnerability. *Environ. Int.* 56, 65–77.
- Barros, V.R., Field, C.B., Dokken, D.J., Mastrandrea, M.D., Mach, K.J., Bilir, T.E., Chatterjee, M., Ebi, K.L., Estrada, Y.O., Genova, R.C., 2014. Climate change 2014 impacts, adaptation, and vulnerability part B: Regional aspects: Working group II contribution to the fifth assessment report of the intergovernmental panel on climate change. In: *Climate Change 2014: Impacts, Adaptation and Vulnerability: Part B: Regional Aspects: Working Group II Contribution to the Fifth Assessment Report of the Intergovernmental Panel on Climate Change*. Cambridge University Press, pp. 1–1820.
- Bernard, J., Bocher, E., Petit, G., Palominos, S., 2018. Sky view factor calculation in urban context: computational performance and accuracy analysis of two open and free GIS tools. *Climate* 6 (3), 60.
- Bradford, K., Abrahams, L., Hegglin, M., Klima, K., 2015. A heat vulnerability index and adaptation solutions for Pittsburgh, Pennsylvania. *Environ. Sci. Technol.* 49 (19), 11303–11311.

- Bröde, P., Fiala, D., Blazejczyk, K., Holmér, I., Jendritzky, G., Kampmann, B., Tinz, B., Havenith, G., 2012. Deriving the operational procedure for the universal thermal climate index (UTCI). *Int. J. Biometeorol.* 56, 481–494.
- Brooks, N., 2003. Vulnerability, risk and adaptation: A conceptual framework. *Tyndall Cent. Climat. Chan. Res. Work. Pap.* 38 (38), 1–16.
- Brown, R., Gillespie, T., 1986. Estimating outdoor thermal comfort using a cylindrical radiation thermometer and an energy budget model. *Int. J. Biometeorol.* 30 (1), 43–52.
- Centers for Disease Control and Prevention, 2019. *Chronic Disease and Health Promotion Data*. <https://chronicdata.cdc.gov/browse?q=PLACES%202021>.
- Chen, T.-L., Lin, H., Chiu, Y.-H., 2022. Heat vulnerability and extreme heat risk at the metropolitan scale: A case study of Taipei metropolitan area, Taiwan. *Urban Clim.* 41, 101054.
- Chen, L., Ng, E., 2012. Outdoor thermal comfort and outdoor activities: A review of research in the past decade. *Cities* 29, 118–125.
- Cheng, W., Li, D., Liu, Z., Brown, R.D., 2021. Approaches for identifying heat-vulnerable populations and locations: A systematic review. *Sci. Total Environ.* 799, 149417.
- Christenson, M., Geiger, S.D., Phillips, J., Anderson, B., Losurdo, G., Anderson, H.A., 2017. Heat vulnerability index mapping for Milwaukee and Wisconsin. *J. Publ. Health Manag. Pract.* 23 (4), 396–403.
- Chuang, W.C., Gober, P., 2015. Predicting hospitalization for heat-related illness at the census-tract level: accuracy of a generic heat vulnerability index in phoenix, Arizona (USA). *Environ. Health Perspect.* 123 (6), 606–612.
- City of Houston, 2020. *City of Houston Users' Guide for Walkable Places and Transit-Oriented Development*. Planning & Development Department.
- Coccolo, S., Kämpf, J., Scartezzini, J.L., Pearlmutter, D., 2016. Outdoor human comfort and thermal stress: A comprehensive review on models and standards. *Urban Clim.* 18, 33–57. <https://doi.org/10.1016/j.uclim.2016.08.004>.
- Conlon, K.C., Mallen, E., Gronlund, C.J., Berrocal, V.J., Larsen, L., O'neill, M. S., 2020. Mapping human vulnerability to extreme heat: a critical assessment of heat vulnerability indices created using principal components analysis. *Environ. Health Perspect.* 128 (9), 097001.
- Correa, E., Ruiz, M.A., Canton, A., Lesino, G., 2012. Thermal comfort in forested urban canyons of low building density. An assessment for the city of Mendoza, Argentina. *Build. Environ.* 58, 219–230.
- Crimmins, A.J., Balbus, J.L., Gamble, C.B., Beard, J.E., Bell, D., Dodgen, R.J., Eisen, N., Fann, M.D., Hawkins, S.C., Herring, L., Jantarasami, D.M., Mills, S., Saha, M.C., Sarofim, J., Trtanj Ziska, L., 2016. The Impacts of Climate Change on Human Health in the United States: A Scientific Assessment, by us Global Change Research Program. U.S. Global Change Research Program. <https://doi.org/10.7930/J0R49NQX>. Retrieved October 01 from.
- Cutter, S.L., Boruff, B.J., Shirley, W.L., 2003. Social Vulnerability to Environmental Hazards. *Social Sci. Q.* 84, 242–261.
- Dastoorpoor, M., Khodadadi, N., Khanjani, N., Borsi, S.H., 2021. Physiological equivalent temperature (PET) index and cardiovascular hospital admissions in Ahvaz, southwest of Iran. *Arch. Environ. Occup. Health* 1–9.
- de Freitas, C.R., Grigorieva, E.A., 2015. A comprehensive catalogue and classification of human thermal climate indices. *Int. J. Biometeorol.* 59 (1), 109–120.
- Eisenman, D.P., et al., 2016. Heat death associations with the built environment, social vulnerability and their interactions with rising temperature. *Health Place* 41, 89–99.
- Ellena, M., Stone, B., Lanza, K., 2019. A methodological assessment of extreme heat mortality modeling and heat vulnerability mapping in Dallas, Texas. *Urban Clim.* 30, 100528 <https://doi.org/10.1016/j.uclim.2019.100528>.
- Ellena, M., Breil, M., Soriani, S., 2020. The heat-health nexus in the urban context: A systematic literature review exploring the socio-economic vulnerabilities and built environment characteristics. *Urban Clim.* 34, 100676.
- Goldie, J., Alexander, L., Lewis, S.C., Sherwood, S.C., Bambrick, H., 2018. Changes in relative fit of human heat stress indices to cardiovascular, respiratory, and renal hospitalizations across five Australian urban populations. *Int. J. Biometeorol.* 62 (3), 423–432.
- Harlan, S.L., et al., 2006. Neighborhood microclimates and vulnerability to heat stress. *Soc. Sci. Med.* 63 (11), 2847–2863.
- Harlan, S.L., et al., 2013. Neighborhood effects on heat deaths: social and environmental predictors of vulnerability in Maricopa County, Arizona. *Environ. Health Perspect.* 121 (2), 197–204.
- Höppe, P., 1999. The physiological equivalent temperature—a universal index for the biometeorological assessment of the thermal environment. *Int. J. Biometeorol.* 43, 71–75.
- Inostroza, L., Palme, M., de la Barrera, F., 2016. A heat vulnerability index: spatial patterns of exposure, sensitivity and adaptive capacity for Santiago de Chile. *PLoS One* 11 (9), e0162464.
- Jayasekara, K., Kulasooriya, P., Wijayasiri, K., Rajapakse, E., Dulshika, D., Bandara, P., Fried, L., De Silva, A., Albert, S., 2019. Relevance of heat stress and dehydration to chronic kidney disease (CKDu) in Sri Lanka. *Prev. Med. Rep.* 15, 100928.
- Johnson, D.P., Stanforth, A., Lulla, V., Lubert, G., 2012. Developing an applied extreme heat vulnerability index utilizing socioeconomic and environmental data. *Appl. Geogr.* 35 (1–2), 23–31.
- Karanja, J., Kiage, L., 2021. Perspectives on spatial representation of urban heat vulnerability. *Sci. Total Environ.* 774, 145634.
- Karimi, M., Nazari, R., Dutova, D., Khanbilvardi, R., Ghandehari, M., 2018. A conceptual framework for environmental risk and social vulnerability assessment in complex urban settings. *Urban Clim.* 26, 161–173.
- Kenny, N.A., Warland, J.S., Brown, R.D., Gillespie, T.G., 2009. Part B: revisions to the COMFA outdoor thermal comfort model for application to subjects performing physical activity. *Int. J. Biometeorol.* 53 (5), 429–441.
- Kenny, N.A., Warland, J.S., Brown, R.D., Gillespie, T.G., 2009a. Part A: Assessing the performance of the COMFA outdoor thermal comfort model on subjects performing physical activity. *Int. J. Biometeorol.* 53 (5), 415–428. <https://doi.org/10.1007/s00484-009-0226-3>.
- Kenny, N.A., Warland, J.S., Brown, R.D., Gillespie, T.G., 2009b. Part B: Revisions to the COMFA outdoor thermal comfort model for application to subjects performing physical activity. *Int. J. Biometeorol.* 53 (5), 429–441.
- Kim, Y., Brown, R., 2021. A multilevel approach for assessing the effects of microclimatic urban design on pedestrian thermal comfort: the high line in New York. *Build. Environ.* 205.
- Kim, Y., Brown, R., 2022. Effect of meteorological conditions on leisure walking: a time series analysis and the application of outdoor thermal comfort indexes. *Int. J. Biometeorol.* 66, 1109–1123.
- Kim, D.W., Deo, R.C., Lee, J.S., Yeom, J.M., 2017. Mapping heatwave vulnerability in Korea. *Nat. Hazards* 89 (1), 35–55.
- Kim, Y., Yu, S., Li, D., Gatson, S.N., Brown, R.D., 2022. Linking landscape spatial heterogeneity to urban heat island and outdoor human thermal comfort in Tokyo: application of the outdoor thermal comfort index. *Sustain. Cities Soc.* 87, 104262 <https://doi.org/10.1016/j.scs.2022.104262>.
- Krstic, N., Yuchi, W., Ho, H.C., Walker, B.B., Knudby, A.J., Henderson, S.B., 2017. The heat exposure integrated deprivation index (HEIDI): a data-driven approach to quantifying neighborhood risk during extreme hot weather. *Environ. Int.* 109, 42–52.
- Kumar, P., Sharma, A., 2020. Study on importance, procedure, and scope of outdoor thermal comfort—A review. *Sustain. Cities Soc.* 61, 102297.
- Kwan, M.P., 2012. The uncertain geographic context problem. *Ann. Assoc. Am. Geogr.* 102 (5), 958–968.
- Lee, Y.-J., 2014. Social vulnerability indicators as a sustainable planning tool. *Environ. Impact Assess. Rev.* 44, 31–42.
- LeSage, James P., 2008. An introduction to spatial econometrics. *Rev. Econ. Ind.* 123, 19–44. <https://doi.org/10.4000/rei.3887>.
- Li, X., Zhang, Y., Li, D., Xu, Y., Brown, R.D., 2022. Ameliorating cold stress in a hot climate: effect of winter storm Uri on residents of subsidized housing neighborhoods. *Build. Environ.* 209, 108646.
- Liang, Jianming, Gong, Jianhua, Sun, Jun, Zhou, Jieping, Li, Wenhong, Li, Yi, Liu, Jin, Shen, Shen, 2017. Automatic Sky View Factor Estimation from Street View Photographs—A Big Data Approach. *Remote Sens.* 9 (5).
- Liang, Jianming, Gong, Jianhua, Zhang, Jinming, Li, Yi, Wu, Dong, Guoyong, Zhang, 2020. GSV2SVF—an interactive GIS tool for sky, tree and building view factor estimation from street view photographs. *Build. Environ.* 168.
- Loughnan, M.E., Tapper, N.J., Phan, T., McInnes, J.A., 2014. Can a spatial index of heat-related vulnerability predict emergency service demand in Australian capital cities? *Int. J. Emerg. Serv.* 3 (1), 6–33.
- Lu, Y., 2019. Using Google street view to investigate the association between street greenery and physical activity. *Landsc. Urban Plan.* 191, 103435.

- Maier, G., Grundstein, A., Jang, W., Li, C., Naeher, L.P., Shepherd, M., 2014. Assessing the performance of a vulnerability index during oppressive heat across Georgia, United States. *Weather, Climat., Soc.* 6 (2), 253–263.
- Maragno, D., Dalla Fontana, M., Musco, F., 2020. Mapping heat stress vulnerability and risk assessment at the neighborhood scale to drive urban adaptation planning. *Sustainability* 12 (3), 1056.
- Marsha, A., et al., 2016. Influences of climatic and population changes on heat-related mortality in Houston, Texas, USA. *Clim. Chang.* 146 (3–4), 471–485.
- Middel, A., Lukaszczuk, J., Zakrzewski, S., Arnold, M., Maciejewski, R., 2019. Urban form and composition of street canyons: A human-centric big data and deep learning approach. *Landscape Urban Plan.* 183, 122–132.
- Morabito, M., Crisci, A., Gioli, B., Gualtieri, G., Toscano, P., Di Stefano, V., et al., 2015. Urban-Hazard Risk Analysis: Mapping of Heat-Related Risks in the Elderly in Major Italian Cities. *PLoS ONE* 10 (5), e0127277.
- Mushore, T.D., Mutanga, O., Odindi, J., Dube, T., 2018. Determining extreme heat vulnerability of Harare Metropolitan City using multispectral remote sensing and socio-economic data. *J. Spat. Sci.* 63 (1), 173–191.
- Nastos, P.T., Matzarakis, A., 2012. The effect of air temperature and human thermal indices on mortality in Athens, Greece. *Theor. Appl. Climatol.* 108 (3), 591–599.
- Nayak, S.G., et al., 2018. Development of a heat vulnerability index for New York state. *Public Health* 161, 127–137.
- Niu, Y., et al., 2021. A systematic review of the development and validation of the heat vulnerability index: major factors, methods, and spatial units. *Curr. Clim. Chan. Rep.* 7 (3), 87–97.
- Ohashi, Y., et al., 2014. Numerical simulations of outdoor heat stress index and heat disorder risk in the 23 wards of Tokyo. *J. Appl. Meteorol. Climatol.* 53 (3), 583–597.
- Oke, T.R., 1981. Canyon geometry and the nocturnal urban heat island: comparison of scale model and field observations. *J. Climatol.* 1 (3), 237–254.
- Openshaw, S., 1981. The Modifiable Areal Unit Problem. *Quantitative Geography: A British View*, pp. 60–69.
- Paelinck, Jean, 1978. *Spatial econometrics*. *Econ. Lett.* 1 (1), 59–63. <https://EconPapers.repec.org/RePEc:eee:ecole:v:1:y:1978:i:1:p:59-63>.
- Potchter, O., et al., 2018. Outdoor human thermal perception in various climates: A comprehensive review of approaches, methods and quantification. *Sci. Total Environ.* 631–632, 390–406.
- Prudent, N., et al., 2016. Assessing climate change and health vulnerability at the local level: Travis County, Texas. *Disasters* 40 (4), 740–752.
- Rainham, D.G., Smoyer-Tomic, K.E., 2003. The role of air pollution in the relationship between a heat stress index and human mortality in Toronto. *Environ. Res.* 93 (1), 9–19.
- Reid, C.E., O’neill, M.S., Gronlund, C.J., Brines, S.J., Brown, D.G., Diez-Roux, A.V., Schwartz, J., 2009. Mapping community determinants of heat vulnerability. *Environ. Health Perspect.* 117 (11), 1730–1736.
- Reid, C.E., Mann, J.K., Alfasso, R., English, P.B., King, G.C., Lincoln, R.A., Woods, B., 2012. Evaluation of a heat vulnerability index on abnormally hot days: an environmental public health tracking study. *Environ. Health Perspect.* 120 (5), 715–720.
- Romero-Lankao, P., et al., 2012. Urban vulnerability to temperature-related hazards: A meta-analysis and meta-knowledge approach. *Glob. Environ. Chang.* 22 (3), 670–683.
- Rossetti, T., Lobel, H., Rocco, V., Hurtubia, R., 2019. Explaining subjective perceptions of public spaces as a function of the built environment: A massive data approach. *Landscape Urban Plan.* 181, 169–178.
- Rundle, A.G., Bader, M.D., Richards, C.A., Neckerman, K.M., Teitler, J.O., 2011. Using Google street view to audit neighborhood environments. *Am. J. Prev. Med.* 40 (1), 94–100.
- Sharma, A., et al., 2018. Role of green roofs in reducing heat stress in vulnerable urban communities—a multidisciplinary approach. *Environ. Res. Lett.* 13 (9).
- Streutker, D., 2003. Satellite-measured growth of the urban heat island of Houston, Texas. *Remote Sens. Environ.* 85 (3), 282–289.
- Sun, Q.C., Macleod, T., Both, A., Hurley, J., Butt, A., Amati, M., 2021. A human-centred assessment framework to prioritise heat mitigation efforts for active travel at city scale. *Sci. Total Environ.* 763, 143033. <https://doi.org/10.1016/j.scitotenv.2020.143033>. Apr 1. Epub 2020 Oct 26. PMID: 33158537.
- Tran, D.N., Doan, V.Q., Nguyen, V.T., et al., 2020. Spatial patterns of health vulnerability to heatwaves in Vietnam. *Int. J. Biometeorol.* 64, 863–872. <https://doi.org/10.1007/s00484-020-01876-2>.
- Uejio, C.K., et al., 2011. Intra-urban societal vulnerability to extreme heat: the role of heat exposure and the built environment, socioeconomic, and neighborhood stability. *Health Place* 17 (2), 498–507.
- United States Census Bureau, 2019. 5-year Estimates from the 2014–2018 American Community Survey (ACS). <https://www.data.census.gov>.
- Vanos, J.K., Warland, J.S., Gillespie, T.J., Kenny, N.A., 2012. Thermal comfort modelling of body temperature and psychological variations of a human exercising in an outdoor environment. *Int. J. Biometeorol.* 56 (1), 21–32.
- Vanos, J.K., Kosaka, E., Iida, A., Yokohari, M., Middel, A., Scott-Fleming, I., Brown, R.D., 2019. Planning for spectator thermal comfort and health in the face of extreme heat: the Tokyo 2020 Olympic marathons. *Sci. Total Environ.* 657, 904–917.
- Yan, H., Fan, S., Guo, C., Wu, F., Zhang, N., Dong, L., 2014. Assessing the effects of landscape design parameters on intra-urban air temperature variability: The case of Beijing, China. *Build. Environ.* 76, 44–53. <https://doi.org/10.1016/j.buildenv.2014.03.007>.
- Yuan, Chao, Chen, Liang, 2011. Mitigating urban heat island effects in high-density cities based on sky view factor and urban morphological understanding: a study of Hong Kong. *Architect. Sci. Rev.* 54 (4), 305–315.
- Zhang, W., Zheng, C., Chen, F., 2019. Mapping heat-related health risks of elderly citizens in mountainous area: a case study of Chongqing, China. *Sci. Total Environ.* 663, 852–866.
- Zheng, M., Zhang, J., Shi, L., Zhang, D., Pangali Sharma, T.P., Prophan, F.A., 2020. Mapping heat-related risks in northern Jiangxi Province of China based on two spatial assessment frameworks approaches. *Int. J. Environ. Res. Public Health* 17 (18), 6584.